

NO-A179 109

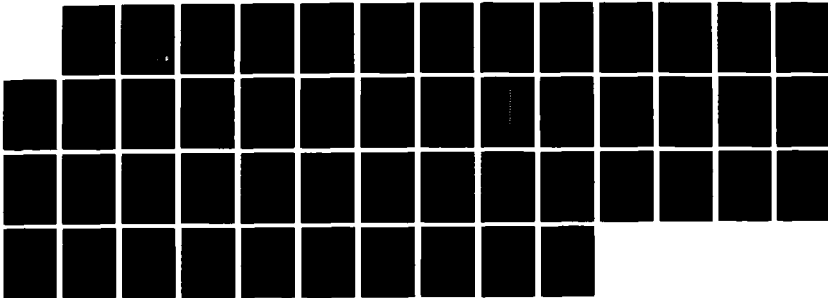
EFFECTS OF LOCAL GEOLOGIC STRUCTURE FOR YUCCA FLATS WTS 1/1
EXPLOSION WAVEFOR. (U) TELEDYNE GEOTECH ALEXANDRIA VA
ALEXANDRIA LABS K L MCLAUGHLIN ET AL. OCT 86 T8AL-86-4

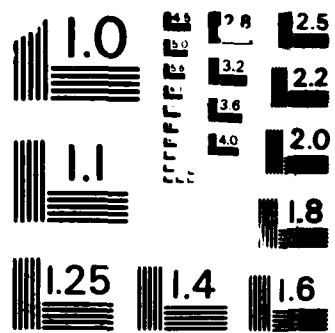
UNCLASSIFIED

AFGL-TR-86-0220 F19620-85-C-0035

F/G 0/11

NL





MICROCOPY RESOLUTION TEST CHART
NATIONAL BUREAU OF STANDARDS - 1963

DTIC FILE COPY

13

AFGL-TR-86-0220

**EFFECTS OF LOCAL GEOLOGIC STRUCTURE
FOR YUCCA FLATS, NTS, EXPLOSION WAVEFORMS:
2-DIMENSIONAL LINEAR FINITE DIFFERENCE SIMULATIONS**

K. L. McLaughlin, L. M. Anderson, and A. C. Lees

Teledyne Geotech Alexandria Laboratory
314 Montgomery Street
Alexandria, Va. 22314.

OCTOBER 1986

SCIENTIFIC REPORT: No. 2

APPROVED FOR PUBLIC RELEASE; DISTRIBUTION UNLIMITED

AIR FORCE GEOPHYSICS LABORATORY
AIR FORCE SYSTEMS COMMAND
UNITED STATES AIR FORCE
HANSCOM AIR FORCE BASE, MASSACHUSETTS 01731

S DTIC
ELECTE **D**
APR 20 1987
E

AD-A179 189

UNCLASSIFIED

SECURITY CLASSIFICATION OF THIS PAGE

REPORT DOCUMENTATION PAGE

Form Approved
OMB No 0704-0188
Exp Date Jun 30, 1986

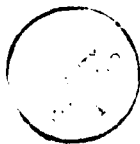
1a REPORT SECURITY CLASSIFICATION Unclassified			1b RESTRICTIVE MARKINGS			
2a SECURITY CLASSIFICATION AUTHORITY			3 DISTRIBUTION/AVAILABILITY OF REPORT Approved for public release; Distribution unlimited			
2b DECLASSIFICATION/DOWNGRADING SCHEDULE						
4 PERFORMING ORGANIZATION REPORT NUMBER(S) - TGAL-86-4 /			5 MONITORING ORGANIZATION REPORT NUMBER(S) AFGL-TR-86-0220			
6a NAME OF PERFORMING ORGANIZATION Teledyne Geotech Alexandria Laboratory		6b OFFICE SYMBOL (if applicable) TGAL	7a NAME OF MONITORING ORGANIZATION Air Force Geophysics Laboratory			
6c ADDRESS (City, State, and ZIP Code) 314 Montgomery Street Alexandria, VA 22314			7b ADDRESS (City, State, and ZIP Code) Hanscom AFB Massachusetts 01731-5000			
8a NAME OF FUNDING/SPONSORING ORGANIZATION Air Force Geophysics Laboratory		8b OFFICE SYMBOL (if applicable) DSO/GSD	9 PROCUREMENT INSTRUMENT IDENTIFICATION NUMBER F19628-85-C-0035			
8c ADDRESS (City, State, and ZIP Code) Hanscom AFB Massachusetts 01731-5000			10 SOURCE OF FUNDING NUMBERS			
		PROGRAM ELEMENT NO 62714E	PROJECT NO 5A10	TASK NO DA	WORK UNIT ACCESSION NO AX	
11 TITLE (Include Security Classification) Effects of Local Geologic Structure for Yucca Flats, NTS, Explosion Waveforms: 2-Dimensional Linear Finite Difference Simulations (Unclassified)						
12 PERSONAL AUTHOR(S) K.L. McLaughlin, L.M. Anderson, and A.C. Lees						
13a TYPE OF REPORT Scientific Report #2		13b TIME COVERED FROM Feb 85 TO Feb 87		14 DATE OF REPORT (Year, Month, Day) October 1986		15 PAGE COUNT 48
16 SUPPLEMENTARY NOTATION						
17 COSATI CODES			18 SUBJECT TERMS (Continue on reverse if necessary and identify by block number)			
FIELD	GROUP	SUB-GROUP				
			Yucca Flats NTS Scattering Linear finite difference P Wave Magnitude			
19 ABSTRACT (Continue on reverse if necessary and identify by block number)						
Two-dimensional linear elastic finite difference calculations were performed for two-dimensional geologic model of Yucca Flats, Nevada Test Site, Nevada. The calculations were used to produce synthetic teleseismic P-wave seismograms for explosive line sources in Yucca Flats. P-wave coda (first 5 seconds) is observed to be highly dependent on takeoff angle for the teleseismic synthetics. P-wave coda varies with the position of the source in the valley structure and may produce variations in the individual station teleseismic P-wave m_b magnitude of up to 0.3 magnitude units. However these magnitude variations should be substantially reduced by averaging over stations at multiple azimuth.						
20 DISTRIBUTION/AVAILABILITY OF ABSTRACT <input checked="" type="checkbox"/> UNCLASSIFIED/UNLIMITED <input type="checkbox"/> SAME AS RPT <input type="checkbox"/> DTIC USERS			21 ABSTRACT SECURITY CLASSIFICATION Unclassified			
22a NAME OF RESPONSIBLE INDIVIDUAL James F. Lewkowicz			22b TELEPHONE (Include Area Code) (617) 861-3028		22c OFFICE SYMBOL LWH	

(19 Continued)

The reverberant coda appears to arise from scattered modal waves that are initially excited in the low velocity near-surface structures of the Yucca Flats deposits of alluvium and tuff. Scattering of the waves occurs at offsets in the basement structure and at the sides of the valley.

The combined effects of scattering, source function, intrinsic attenuation, and instrument response serve to obscure the expected P+pP spectral scalloping that is expected from a linear model. This loss of spectral resolution is the product of P coda filling in the P+pP interference notches and the lengthening of the initial P wave source time function by the convolution of the source time function, intrinsic attenuation operator and instrument response. Therefore, short time windows that do not include P coda energy do not have sufficient resolution to reliably detect the P+pP interference notches.

Accession For	
NTIS GRA&I	<input checked="" type="checkbox"/>
DTIC TAB	<input type="checkbox"/>
Unannounced	<input type="checkbox"/>
Justification	
By _____	
Distribution/	
Availability Codes	
Dist	Avail and/or Special
A-1	



**EFFECTS OF LOCAL GEOLOGIC STRUCTURE
ON YUCCA FLATS, NTS, EXPLOSION WAVEFORMS:
2-DIMENSIONAL LINEAR FINITE DIFFERENCE SIMULATIONS**

SUMMARY

Two-dimensional linear elastic finite difference calculations were performed for a two-dimensional geologic model of Yucca Flats, Nevada Test Site, Nevada. The calculations were used to produce synthetic teleseismic P-wave seismograms for explosive line sources in Yucca Flats. P-wave coda (first 5 seconds) is observed to be highly dependent on takeoff angle for the teleseismic synthetics. P-wave coda varies with the position of the source in the valley structure and may produce variations in the individual station teleseismic P-wave m_b magnitude of up to 0.3 magnitude units. However these magnitude variations should be substantially reduced by averaging over stations at multiple azimuths.

The reverberant coda appears to arise from scattered modal waves that are initially excited in the low velocity near-surface structures of the Yucca Flats deposits of alluvium and tuff. Scattering of the waves occurs at offsets in the basement structure and at the sides of the valley.

The combined effects of scattering, source function, intrinsic attenuation, and instrument response serve to obscure the expected P+pP spectral scalloping that is expected from a linear model. This loss of spectral resolution is the product of P coda filling in the P+pP interference notches and the lengthening of the initial P wave

source time function by the convolution of the source time function, intrinsic attenuation operator and instrument response. Therefore, short time windows that do not include P coda energy do not have sufficient resolution to reliably detect the P+pP interference notches.

INTRODUCTION

Yucca Flats explosion waveforms have often been noted to possess unusual reverberant P coda. The suggestion that this complication is due to near-source structure is apparent from observations that teleseismic P coda recorded in Yucca Flats is also reverberant (Der et al 1980). Also, regional phases such as Pg and Lg recorded in Yucca Flats are anomalously large and have extended codas (Der et al 1980).

Also, several authors have claimed that there are systematic magnitude anomalies due to location within Yucca Flats (Blandford and et al, 1977; Minster et al, 1981; Ferguson, 1981, 1983; Mellman et al 1983). These magnitude anomalies have generally been associated with the shallow graben structure of Yucca Flats. The horst and graben structures strike north-south and magnitude anomalies have generally been attributed to the east west lateral variation in structure.

We present simulations of explosions within the laterally varying structure of Yucca Flats. The calculations are 2-D linear elastic finite difference calculations for line sources in a 2-D model. The calculations are used to simulate the first 5 seconds of teleseismic P waveforms. Variations in m_b and P-coda are observed as a function of take-off angle and azimuth. Spectra of the teleseismic waveforms are also examined. We compare the waveforms predicted from the 2-D modeling with waveforms

predicted from simple 1-D layered models. Finally we show some deconvolved equivalent source time functions of Yucca Flats explosions at the arrays EKA, YKA, and GBA as well as recordings at the LRSM station, RK-ON.

CALCULATIONS

A 2-D geologic structure suggested by Ferguson (1981, 1983) was used to calculate synthetic seismograms for explosion sources in Yucca Flats. The structure is shown in Figure 1 with a 5-to-1 vertical exaggeration. The structure can be considered to be a West-to-East cross-section, looking North along the strike of the valley. The upper most layer has a P-wave velocity of 1.34 km/sec, and represents the surface alluvial deposits that cover the valley floor. The intermediate depth layer has a P-wave velocity of 2.14 km/sec and represents a layer of undersaturated tuffs. The 3.0 km/sec layer represents the saturated tuffs that unconformably overlay the 4.57 km/sec Paleozoic carbonate sediments that form what is usually referred to as the Paleozoic basement. The basement itself has been folded and faulted in the Cenozoic. Faulting is primarily responsible for the basement relief shown in Figure 1, but a pre-volcanic (Tertiary) erosional surface provides some of the basement relief. Review and summary of the Geology of Yucca Flats may be found in Barnes, Housner, and Poole (1963), Barnes and Poole (1968), Colton and McKay (1966), Keller (1960), Ekren (1968), and Ramspott and Howard (1975).

The S-wave velocity (β) was assumed to be directly related to the P-wave velocity (α) by the following linear relationships: for $\alpha < 3.0$, $\beta = 0.45 \alpha$; for $3.0 < \alpha < 5.0$, $\beta = 0.50 \alpha$; and for $\alpha > 5.0$, $\beta = 0.59 \alpha$. The 2-D linear elastodynamic finite

difference calculations (Kelley et al 1976) were performed on a grid with 0.05 km spacing. A two point radius smoothing operator was applied to the model in Figure 1 in order to smooth the first order discontinuities. Consequently the first order discontinuities in Figure 1 are replaced by gradient layers 2 to 3 grid spaces thick (100 to 150 meters). A broadband plane P-wave pulse was directed from the 4.57 km/sec half-space at either a normal, 5 , 10, or 15 degree incidence angle. A flat free-surface boundary condition was assumed for the top of the grid, and the Clayton and Engquist (1977) absorbing boundary conditions were used for the sides and bottom of the grid. The dilatation was computed at each of the numbered sites indicated in Figure 1, at a depth of 550 meters in the saturated tuff layer. By use of the reciprocity principle, the displacement response at an infinite distance (teleseismic) was determined for a dilatational line source with a von-Seggern and Blandford (1972) reduced displacement potential (RDP). The RDP was appropriate for a 100 Kt explosion in hard rock. A frequency dependent attenuation operator appropriate for NTS to shield path (Der and Lees, 1984) (see Figure 2) and an instrument response were then applied to the final synthetic seismogram. The synthetic seismograms are considered accurate up to 4 Hz. At frequencies above 4 Hz, the S-wave wavelengths are shorter than 10 grid spaces in the slowest portions of the model. Since 4 Hz P waves are rarely seen at teleseismic distances from NTS, this is not considered an important limitation. Incidence angles of 0, 5, 10, and 15 degrees (in the 4.57 km/sec halfspace) were used so that the P-wave synthetics correspond to teleseismic P-wave slownesses of 0.0 2.0, 4.0, and 6.4 sec/km. Flat layered models for the same incidence angles were calculated to compare with the 2-D model of Figure 1. These flat layered models were chosen to coincide

with the vertical velocity sections of Figure 1 at source points 5 and 10.

Figure 3 shows seismograms for a takeoff angle of 15 degrees at the numbered source locations 1 through 13 in Figure 1. Five seconds of synthetic seismograms are shown. All traces are shown at the same relative scale. The takeoff angle is defined such that the receiver is to the east of the valley at a distance of 65 degrees. Note that the initial P waveform is fairly stable with the characteristic P+pP interference notch while the coda varies dramatically across the model. The coda appears to be larger for sources towards the west.

For comparison, Figure 4 shows the seismograms for source locations 7, 8, and 9 at takeoff angles of 15 and -15 degrees (receivers to the east and west respectively). Additionally, the response of a 1-D layered model for the same takeoff angle is shown. All seismograms are shown at the same scales. The coda of the 1-D layered model is much reduced while the initial P waveform is very similar to that of the 2-D model. The receiver to the west (-15 degrees) has a slightly different P+pP interference notch and slightly less coda.

To further demonstrate the P-coda generation inherent in the 2-D model, Figure 5 shows the response of the 2-D model for a takeoff angle of 15 degrees, and sources at locations 4, 5, and 6 compared to the response of a 1-D model with the same vertical velocity structure as at source location 5. The principle differences remain in the P coda following the P wave by more than 2 seconds.

The 1-D vertical velocity structures of Yucca Flats taken at source locations 5 and 10 produce very similar responses as seen in Figure 6. The seismograms are off-

set slightly for the comparison. Simple 1-D layered models do not produce sizable anomalies in the teleseismic seismogram.

The coda generation appears to be a strong function of the takeoff angle. Figure 7 shows the response of the model for a source at location 5, and takeoff angles of 0 and 15 degrees. The P wave of zero slowness has much reduced coda generation. However, the initial P waveform is similar for the two takeoff angles.

AMPLITUDE SPECTRA

Figure 9 shows amplitude spectra for a source at location 7 and takeoff angles of 0, 5, 10, and 15 degrees. A 2.5 second window has been used for each spectral estimation. No smoothing operator has been applied. No source time function, seismometer response, or attenuation operator has been applied to the model response. The P+pP interference notches are clearly visible for all takeoff angles. The structure explored here is not sufficiently complex to obscure the linear pP reflection viewed at teleseismic distances.

Figures 9A and 9B show spectra for 2.5 and 5.0 second windows for the source location 5, takeoff angles 15 and -15 degrees with source time function, seismometer response, and attenuation operator applied to the model response. The P+pP spectral scalloping is no longer apparent in the spectra. Figure 9C shows the spectra for a 1-D layered model. The P+pP spectral modulation is evident in the 1-D layered model spectra for both the 2.5 and the 5.0 second windows. Therefore, the 2-D model is responsible for the lack of P+pP spectral modulation when the source time function, attenuation operator, and instrument response have been convolved with the model

response. Since the model response without the complications of source, attenuation, and instrument shows P+pP nulls for short windows, it is evident that the smearing effects of the convolution also contributes to the loss of spectral resolution.

TELESEISMIC m_b

In order to compare the predicted magnitude anomaly that may occur for a laterally varying model such as this, the amplitudes of the "a", "b", and "max" phase of the P waves of Figure 3A and B were measured and plotted in Figures 10A, 10B, and 10C. The variation is plotted as $\log(\text{amplitude})$ and $\log(\text{amplitude}/\text{period})$ just as teleseismic magnitudes are computed. The $\log(A)$ and $\log(A/T)$ measurements are shown West-to-East across the model at source locations 1-to-13 in Figure 1. The "a", and "b" phase measurements show little variation as expected. Maximum variation is 0.20 magnitude units for $m_b(P_a)$ and $m_b(P_b)$. The $m_b(P_a)$ and $\log(A)$ measurements show slightly less variation than the $m_b(P_b)$ and $\log(A/T)$ measurements. The $m_b(P_{\text{max}})$ measurements show the greatest variation since they are dominated by the later coda for several synthetic seismograms. The range of $\log(P_{\text{max}}/T)$ variation is at most 0.4 magnitude units. $\log(P_{\text{max}}/T)$ has a larger variation than $\log(P_{\text{max}})$. Obviously, the estimation of the dominant period, T, is a significant source of estimation or measurement error. Since network standard deviations of 0.3 to 0.4 magnitude units are typical for single stations, it is conceivable that at least part of the variation of $\log(P_{\text{max}})$ may be the early P coda generation by the laterally varying structure. Standard procedures for measuring m_b require that the largest arrival in the first few seconds be used for measurement. A higher $\log(P_{\text{max}})$ magnitude is observed for

source locations 1 and 2 on the western side of the Yucca Flats structure. A $\log(P_{\max})$ magnitude minima occurs in the center of the Flats structure and the pattern is similar to the pattern found by Mellman et al. (1983), although the amplitude of the predicted fluctuation appears to be 0.2 magnitude units larger in this study.

COMPARISON WITH OBSERVED WAVEFORMS

The P-coda arises from the scattering of waves initially excited in the low velocity graben structure of the valley. Fault offsets and slopes of the basement act as locations for the conversion of the trapped waves into downward propagating P-waves. In the case of our 2-D simulations, these trapped waves are excited by a line source and propagate in a 2-D structure, and therefore they have less geometrical spreading than do waves from a point source in a 3-D structure. In fact, Rayleigh waves under these 2-D circumstances do not attenuate with distance if it were not for scattering. Therefore, P-coda is probably over estimated by the 2-D calculations. The P-coda predicted by our 2-D calculations should constitute a good upper bound to the P-coda generated by explosions in Yucca Flats.

We show in Figure 11A deconvolved source time functions (see Shumway and Der, 1985) Yucca Flats shots and Piledriver (Climax Stock) recorded at EKA (71.4°). The resolution kernel for the deconvolution is shown at the top of Figure 11A and indicates the potential resolution afforded by the bandwidth of the deconvolution, 0.4 to 3.5 Hz. The instrument and frequency independent $t^*=0.45$ sec attenuation operator have been removed as part of the multichannel deconvolution. See Table 1 for event information. The Yucca Flats explosion source time functions (far-field displacement)

show reverberation lasting several seconds. Piledriver was detonated in the Climax Stock located to the north of Yucca Flats and does not show the low-frequency reverberation. Although Piledriver shows a negative polarity pulse following the initial P wave by about 0.25 seconds that could be interpreted as a pP, the Yucca Flats events show little or no apparent pP's within 1 seconds following the initial P wave.

We argue that the major variations in the elements of the "equivalent source functions" presented are due to the near source structure. Topgallant and Strait were located only 0.36 km apart. Likewise Lowball and Hearts were located 1.32 km apart. There are a number of similarities between the "equivalent source functions" for these two pairs of records. Lowball and Hearts were located between 2 and 2.25 km from Topgallant and Strait and the two pairs of explosion time functions show systematic differences. Farallones is located more than 4 km from any other explosion shown in Figure 11A and looks the least like any of the other explosions.

Figure 11B shows deconvolved source time functions for seven Yucca Flats events at YKA (25.5°) but the records are complicated by the upper mantle triplications. The first triplication lengthens and complicates the source time function considerably. The second triplication is prominent about 16 seconds following the initial P wave. Again, similarities between pairs of equivalent source time functions are apparent for explosions that were located close together. Scantling and Topgallant were separated by 0.45 km, Quargel and Cabrillo by 0.79 km, Crewline and Lowball by 1.74 km and Crewline and Bulkhead by 1.51 km. Many of the fine details of the coda and the two triplications can be correlated between pairs of neighboring events.

Figure 11C shows three out of four events at GBA (127.8°) that exhibit the reverberant P-coda in the first 5 seconds. Also, it is apparent that the near source generated coda is azimuthally dependent when Strait at GBA is compared to Strait at EKA. The explosion pairs Crewline and Bulkhead and Crewline and Strait are separated by 1.51 and 1.59 km respectively. Farallones on the other hand is located more than 4 km from any of the the other events in Figure 11C.

The individual traces of the R3 element of the EKA array are shown for 5 Yucca Flats events and Piledriver (as in Figure 11A). The source complexity is still apparent in these raw records when we compare Piledriver to the Yucca Flats events.

Figure 13 shows the complexity of several Yucca Flats events compared to Piledriver at the station RK-ON (Table 1 for event information). The reverberant P coda is clearly due to near-source structure since the Piledriver record shows much less complexity and the paths are nearly identical except for the Yucca Flats, Climax Stock locations in NTS. The only pair of explosions located within 1 km of each other in Figure 13 are Chiberta and Commodore, and they show similarities in the coda out to P+20 seconds..

These records make a qualitative argument that much of the equivalent source time function observed teleseismically from Yucca Flats explosions is near source related and varies with azimuth and location within the Valley.

TABLE 1. EVENT LOCATIONS AND DEPTHS					
YEAR	DOY	EVENT	LAT.	LONG.	DEPTH(km)
1966	153	PILED RIVER	37.22707	-116.05554	0.4627
1967	140	COMMODORE	37.13041	-116.06395	0.7452
1975	059	TOPGALLANT	37.10620	-116.05625	0.7132
1975	066	CABRILLO	37.13401	-116.08424	0.6005
1975	114	EDAM	37.11568	-116.08739	0.4115
1975	120	OBAR	37.10886	-116.02880	0.5690
1975	154	MIZZEN	37.09483	-116.03610	0.6370
1975	249	MARSH	37.02365	-116.02831	0.4267
1975	354	CHIBERTA	37.12765	-116.06157	0.7160
1976	077	STRAIT	37.10728	-116.05247	0.7803
1977	117	BULKHEAD	37.09479	-116.02789	0.5943
1977	145	CREWLINE	37.09433	-116.04486	0.5639
1977	231	SCANTLING	37.11003	-116.05451	0.7010
1977	348	FARALLONES	37.13587	-116.08603	0.6680
1978	193	LOWBALL	37.07867	-116.04379	0.5639
1978	322	QUARGEL	37.12687	-116.08388	0.5420
1979	249	HEARTS	37.08811	-116.05279	0.6400

CONCLUSIONS

We show that the reverberant P-coda from Yucca Flats explosions is due to the scattering of trapped waves in the low-velocity structure by variations in the Paleozoic basement of the horst and graben structure. This reverberation can be seen at a number of azimuths (Mellman et al 1983) and clearly distinguishes Yucca Flats explosions from Pahute Mesa or Climax Stock explosions. We find that the P-coda increases with increasing takeoff angle.

Variations in individual seismic station m_b (P_{max})'s may approach 0.3 magnitude units due to changes in location of the explosion, takeoff angle, and azimuth. However, these variations should be reduced substantially by network averaging.

Neither the m_b (Pmax) variations nor the P-coda variations can be attributed to a purely 1-D layered structure without lateral variation. Although our calculations agree favorably with Haskell-Thompson calculations for 1-D layered structures, there are no independent checks of the calculations for full elastic calculations of line sources in 2-D models. Because of the differences between 2-D and 3-D calculations, the P-coda predicted by these methods is probably an upper bound on the true 3-D case. Observations of Yucca Flats explosions do show the reverberant P-coda at several azimuths.

It was found that although there is an elastic P+pP scalloping in the spectra of the model response, that when instrument, source, and attenuation operators were convolved with the model response, that there is a "smearing" effect that diminishes the resolution of the interference notches. The P+pP time function is drawn out into the P-coda by the convolutions and the P-coda tends to fill in the interference notches. These simulations point out the difficulty of observing such notches in the spectra of a signal. A short window with poor spectral resolution is required to observe the notches but a long window with higher spectral resolution includes P-coda that contaminate the elastic P+pP scalloping.

We do not require complicated sources to simulate the Yucca Flats reverberant seismograms. The initial portion of the waveform is the least altered by propagation in the structure. We see no mechanism for apparent \bar{r}^* differences due to the scattering of waves in the Yucca Flats structure. We predict that deterministic m_b variations should be expected as a function of location within Yucca Flats. The m_b variations are best treated by suitable averaging over numerous azimuths around the source.

ACKNOWLEDGEMENTS

This work was supported under Contract F19628-85C-0035, administered by the Air Force Geophysics Laboratory. The views and conclusions contained in this report are those of the authors and should not be interpreted as representing the official policies, either expressed or implied, of the Defense Advanced Research Projects Agency or the U.S. Government.

REFERENCES

- Barnes, H., F. N. Housner, and F.G. Poole (1963) Geology of the Oak Spring Quadrangle, Nye County, Nevada.
- Barnes, H. and F. G. Poole (1968) Regional thrust-fault system in Nevada Test Site and vicinity, *GSA 110*, 233-238.
- Barker, B.W., Z. A. Der, and C. P. Mrazek (1980) The effects of crustal structure on the regional phases Pg and Lg at the Nevada test site. *J. Geophys. Res.*, 86, 1686-1700.
- Blandford, R. R. M. F. Tillman, and D. Racine (1977) Empirical mb:Ms relations at the Nevada Test Site with applications to mb:yield relations *Teledyne Geotech Report, SDAC-TR-76-14*. Alexandria, Va. 22314.
- Clayton, R. and B. Engquist (1977). Absorbing boundary conditions for acoustic and elastic waves equations, *Bull. Seism. Soc. Am.* 67, 1529-1540.
- Colton, R. B., E. J. McKay (1966) Geologic Map of the Yucca Flat Quadrangle, Nye County, Nevada.
- Ekren, E. B. (1968) Geologic setting of Nevada Test Site and Nellis Air Force Range, *GSA 110*, 5-10.
- Ferguson, J. F. (1981) Geophysical investigations of Yucca Flat, Nevada, Ph.d Thesis, So. Methodist Univ., Dallas, TX 75275.
- Ferguson, J. F. (1983) AFOSR Semi-Annual Report, Southern Methodist Univ., Dallas, TX 75275.
- Keller, G. V. (1960) Physical properties of the Oak Springs Formation, Nevada, USGS Prof. Paper B 396-400.
- Kelly, K. R., R. W. Ward, S. Treitel, and R.M. Alford (1976), Synthetic seismograms, a finite difference approach. *Geophysics*, 41, 2-27.
- Minster, J. B., J. M. Savino, W. L. Rodi, T. H. Jordan, J. F. Masso (1981) Three-dimensional velocity structure of the crust and upper mantle beneath the Nevada Test Site, *Systems Science and Software, Final Report SSS-R-81-5138*, La Jolla, Calif. 92038.
- Mellman, G. R., R. S. Hart, G. M. Lundquist, and D. M. Hadley (1983) Investigations of near-source structural effects on body waves, Part I - Yucca Flats receiver functions appropriate to NTS; motive functional specifications, *Sierra Geophysics Report SGI-R-82-058*, Redmond, Washington 98052.
- Ramspott, L. D. and N. W. Howard (1975) Average properties of nuclear test areas and media at the USERDA Nevada Test Site, UCRL-519348, Lawrence Livermore Laboratory, Livermore Calif. 94550.

Shumway, R. A., and Z. A. Der (1985). Deconvolution of multiple time series, *Technometrics*, 27, 385-393.

von Seggern D. H. and R. R. Blandford (1972) Source time functions and spectra for underground nuclear Explosions, *Geophys. J. Roy. Astr. Soc.*, 31, 83-97.

FIGURE CAPTIONS

FIGURE 1. West-to-East model for geologic structure across Yucca Flats from Ferguson (1983). Model shown with 5-to-1 vertical exaggeration. Numbered source locations referred to in the text are indicated by solid dots at a depth of 550 meters below the surface. P-wave velocities of 1.34, 2.14, 3.00, and 4.57 km/sec are indicated for the geologic units of alluvium, unsaturated tuff, saturated tuff, and Paleozoic carbonates respectively.

FIGURE 2. Frequency dependent $t^*(f)$ for NTS to shield path from Der and Lees (1985). Time domain attenuation operator, $A(t)$, is shown as inset. \bar{r}^* is 0.45 seconds at 1 Hz.

FIGURE 3A, 3B. Teleseismic P-wave synthetics appropriate for a takeoff angle of 15 degrees for model in Figure 1. Numbers correspond to numbered source locations in Figure 1. 5 seconds of record are shown in each case. All synthetics are plotted at the same scale. Synthetics are calculated for a von Seggern Blandford (1972) hard rock 100 Kt RDP convolved with an instrument response and an attenuation operator as in FIGURE 2.

FIGURE 4. Synthetics for the Yucca Flats model at source locations 7, 8, and 9, for takeoff angles of 15 and -15 degrees. Right-most seismograms are for a 1-D layered model and a takeoff angle of 15 degrees.

FIGURE 5A. Synthetics for source locations 4, 5, and 6 at takeoff angle of 15 degrees compared to the layered model.

FIGURE 5B. Comparison of linear elastic finite difference calculations with results of a Haskell-Thompson matrix solution for the layered structure at the source location 5. Takeoff angle is 15 degrees.

FIGURE 5C. Spectra of the two traces seen in FIGURE 5B.

FIGURE 6. Synthetics for 1-D layered models at source locations 5 and 10. Takeoff angle is 15 degrees.

FIGURE 7. Synthetics for the 2-D Yucca model, source location 5, at normal and 15 degree takeoff angles.

FIGURE 8. 2.56 second spectra of P waves for 0, 5, 10, and 15 degree takeoff angle, source location 7. P+pP interference pattern is clearly visible in all spectra. Spectra do not have the source, attenuation, and instrument responses convolved with the model response as in previous Figures.

FIGURE 9A,B,C. 2.5 and 5.0 second windows of the synthetics for source location 5 with takeoff angles of 15 (9A) and -15 (9B) degrees. (9C) shows the spectra for a 1-D layered structure appropriate for the same source location.

FIGURE 10A. $\log(A)$ and $\log(A/T)$ for "a" phase of the P wave synthetics with a 15 degree takeoff angle. Numbers refer to source locations in Figure 1. Maximum variation is 0.15 log units.

FIGURE 10B. $\log(A)$ and $\log(A/T)$ for "b" phase of the P wave synthetics with a 15 degree takeoff angle. Source locations 1 through 13 in Figure 1. Maximum variation

is 0.15 log units.

FIGURE 10C. $\log(A)$ and $\log(A/T)$ for "max" phase of the P wave synthetics with a 15 degree takeoff angle. Source locations 1 through 13 in Figure 1. Maximum variation is 0.3 log units.

FIGURE 11A. Deconvolved source time functions (far-field displacement) of Yucca Flats events and Piledriver at EKA array ($\Delta=71.4^\circ$). The effects of a constant $t^*=0.45$ sec attenuation operator have been removed. A resolution kernel is shown at the top representing the limited bandwidth of the deconvolutions, 0.4 to 3.5 Hz. The initial causal P wave has been shaded for clarity. Note the higher frequency and shorter duration source time function of Piledriver with respect to the Yucca Flats events. Topgallant, Lowball, and Farallones have considerable reverberation in the first 5 seconds of record. The Yucca Flats events do not show a clear pP within 1 second of the initial P wave, although several events do show a negative phase about 1 second following the P wave and positive and a positive pulse about 1.5 seconds following the P wave. Piledriver shows a negative pulse about 0.25 seconds following the P wave (pP?) and another negative polarity pulse about 0.8 seconds following the P wave.

FIGURE 11B. Deconvolved source time functions (far-field displacement) of Yucca Flats events at YKA array ($\Delta=25.5^\circ$). The effects of a constant $t^*=0.45$ sec attenuation operator have been removed. A resolution kernel is shown at the top representing the limited bandwidth of the deconvolutions, 0.4 to 3.5 Hz. The initial causal P wave has been shaded for clarity. The P waves are doubly triplicated at this distance range. The initial P wave (shaded) is followed by a second stronger P wave by about 1.3 to 1.5 second. The two arrivals constructively interfere to produce a reverberant waveform that lasts 8 seconds or more. A second P-wave triplication follows the initial P waves by about 16 seconds.

FIGURE 11C. Deconvolved source time functions (far-field displacement) of Yucca Flats events at GBA array ($\Delta=127.8^\circ$). The effects of a constant $t^*=0.45$ sec attenuation operator have been removed. A resolution kernel is shown at the top representing the limited bandwidth of the deconvolutions, 0.4 to 3.5 Hz. The initial causal P wave has been shaded for clarity. Strait, Crewline and Bulkhead show the characteristic reverberation of Yucca Flats events. Azimuthal differences are apparent if we compare Strait and Farallones between GBA and EKA (FIGURE 11A).

FIGURE 12. The individual traces of the R3 element of the EKA array are shown for 5 Yucca Flats events and Piledriver (as in Figure 11A). The source complexity is less apparent in these raw records when we compare Piledriver to the Yucca Flats events. The multichannel deconvolutions of Figure 11A improve the signal-to-noise over the single trace records.

FIGURE 13. Several Yucca Flats events recorded at RK-ON ($\Delta=21.0^\circ$) compared to Piledriver. Note the complexity of the P coda from the Yucca Flats events. Complexity is not due to receiver structure or upper mantle P wave complications, but must be due to the near-source structures of the Yucca Flats events. Chiberta and Commodore were located only 0.37 km apart.

YUCCA 1

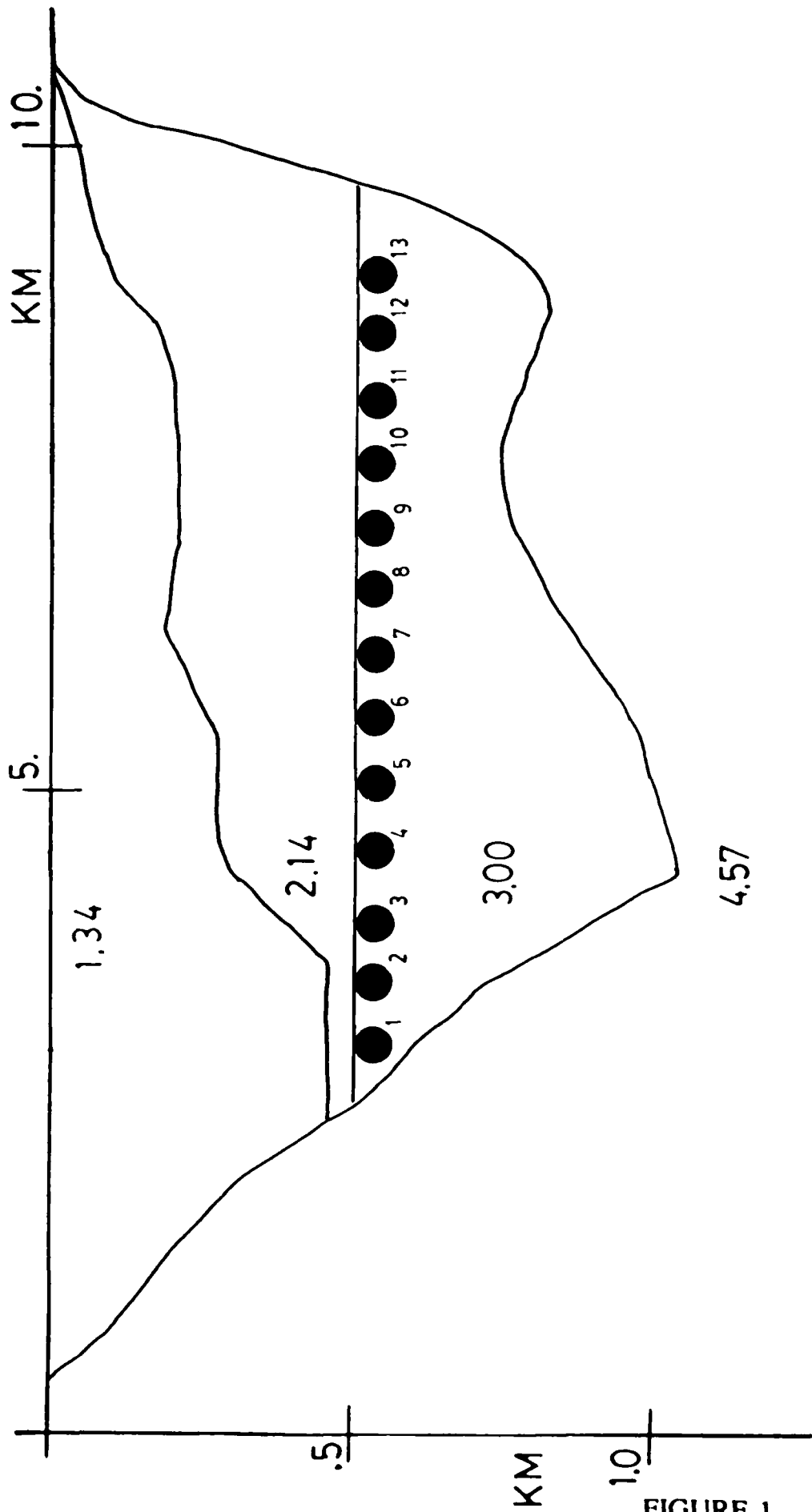
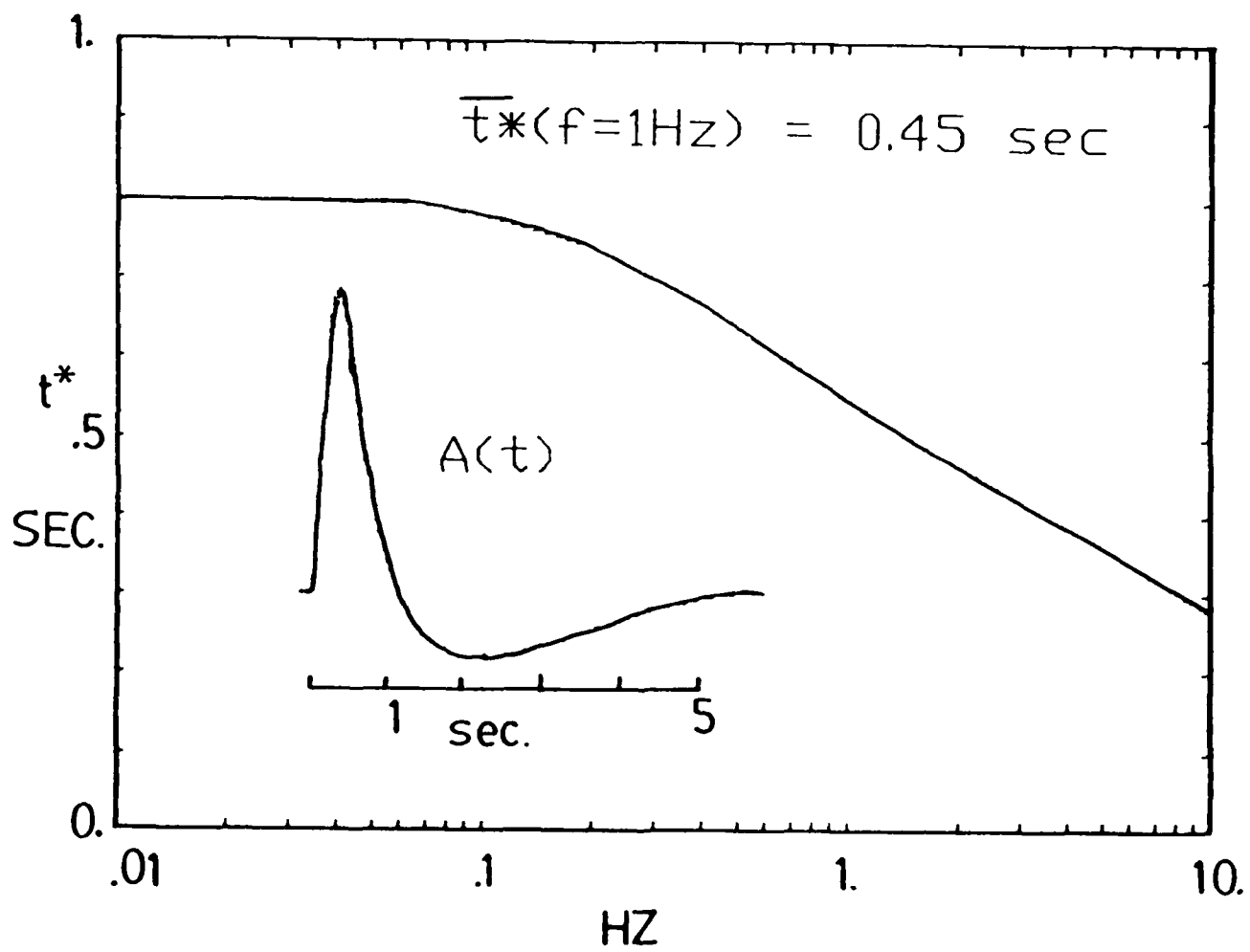
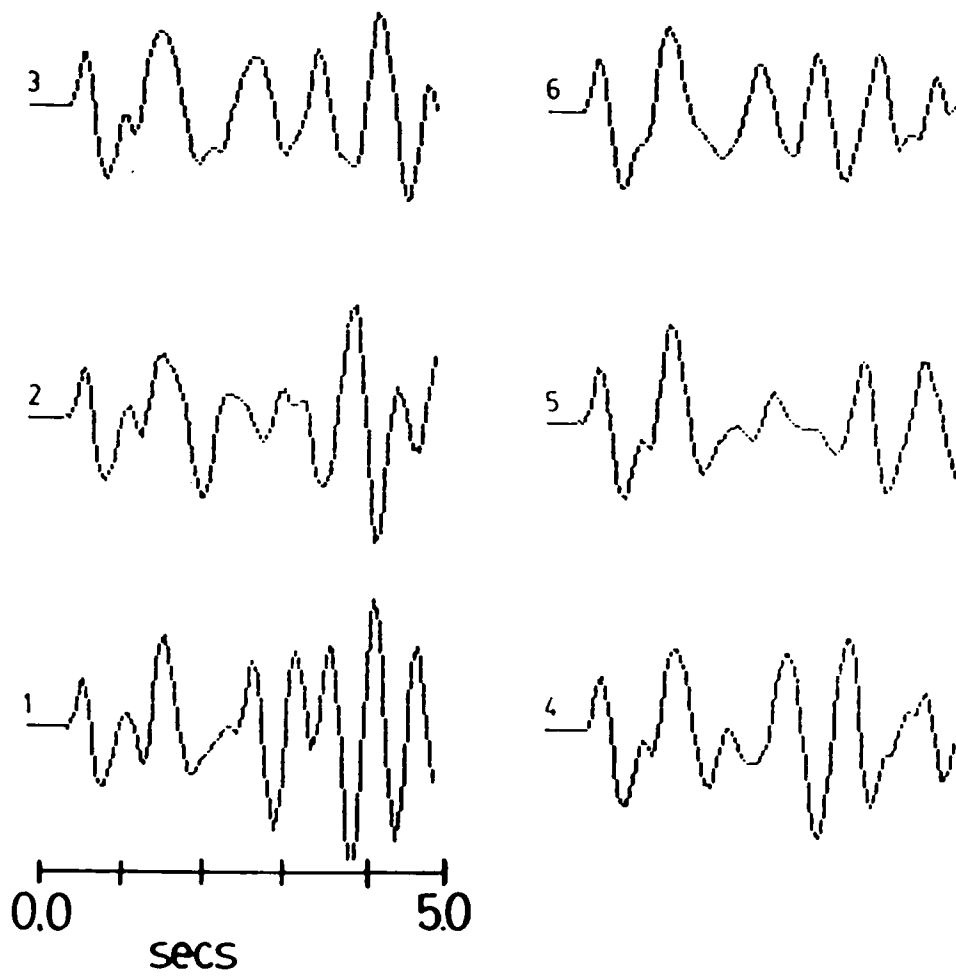
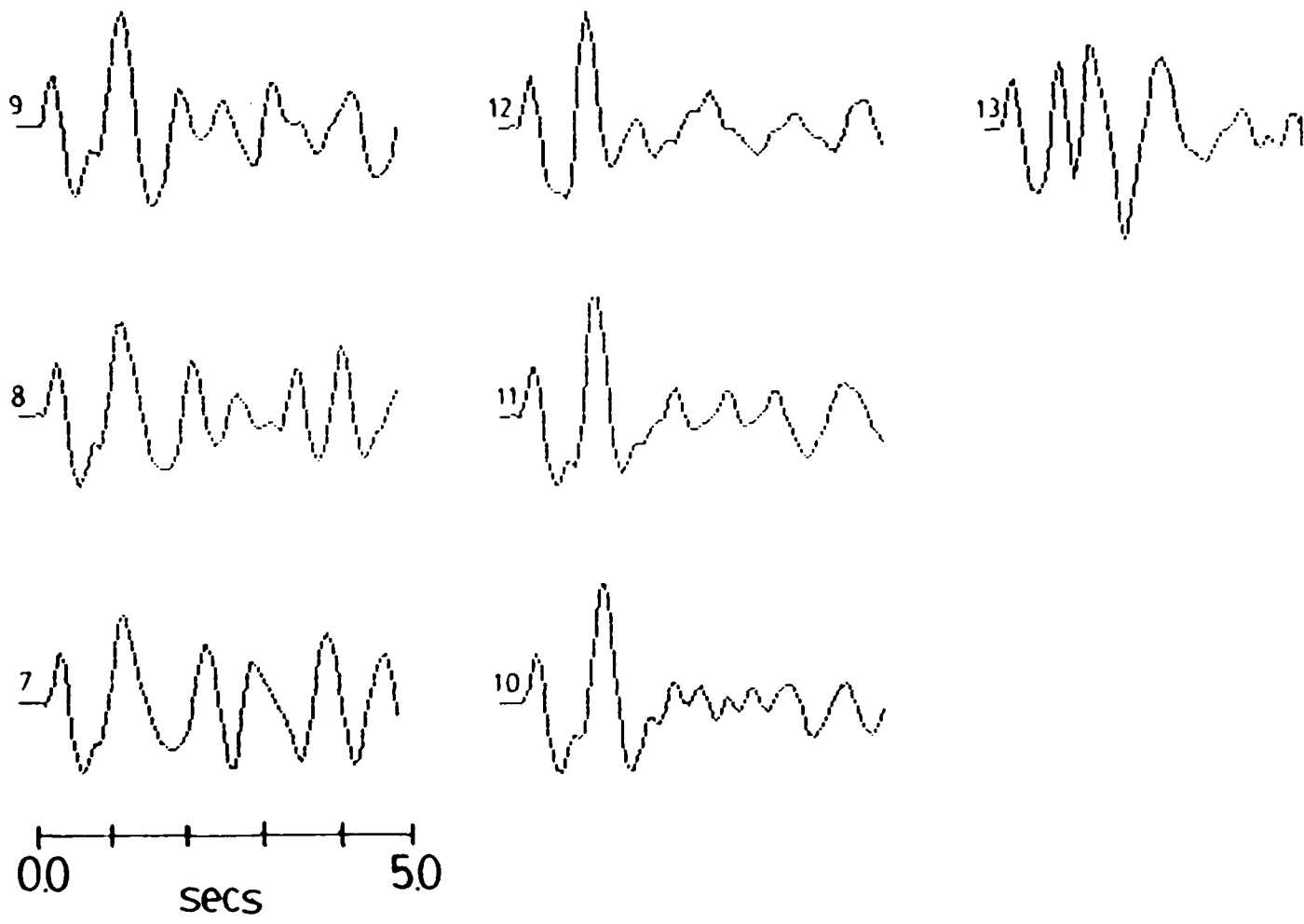


FIGURE 1



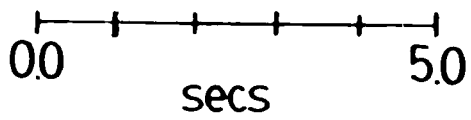
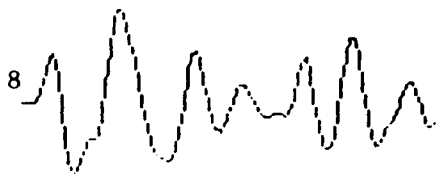


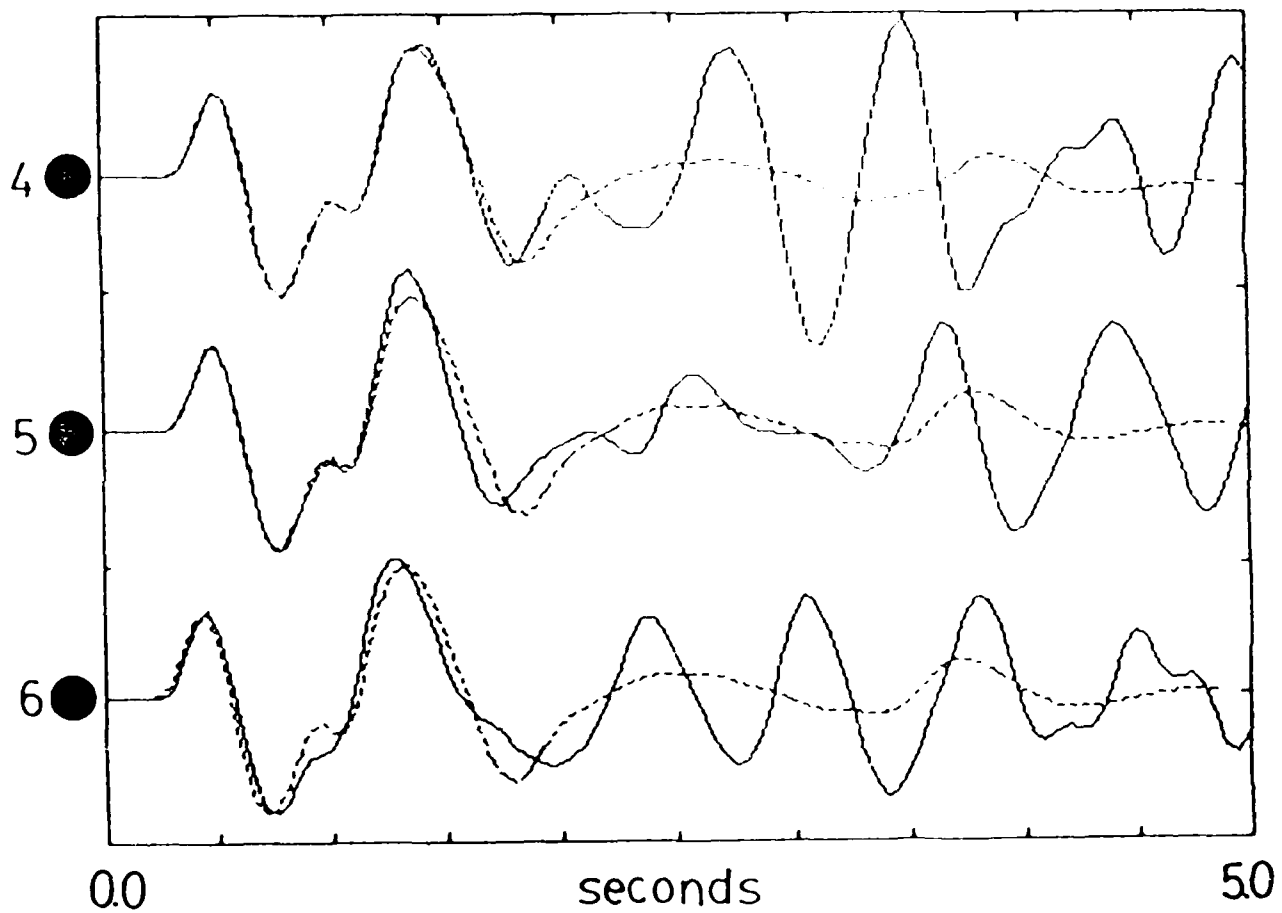


YUCCA 1
 $\angle = 15^\circ$

YUCCA 1
 $\angle = 15^\circ$

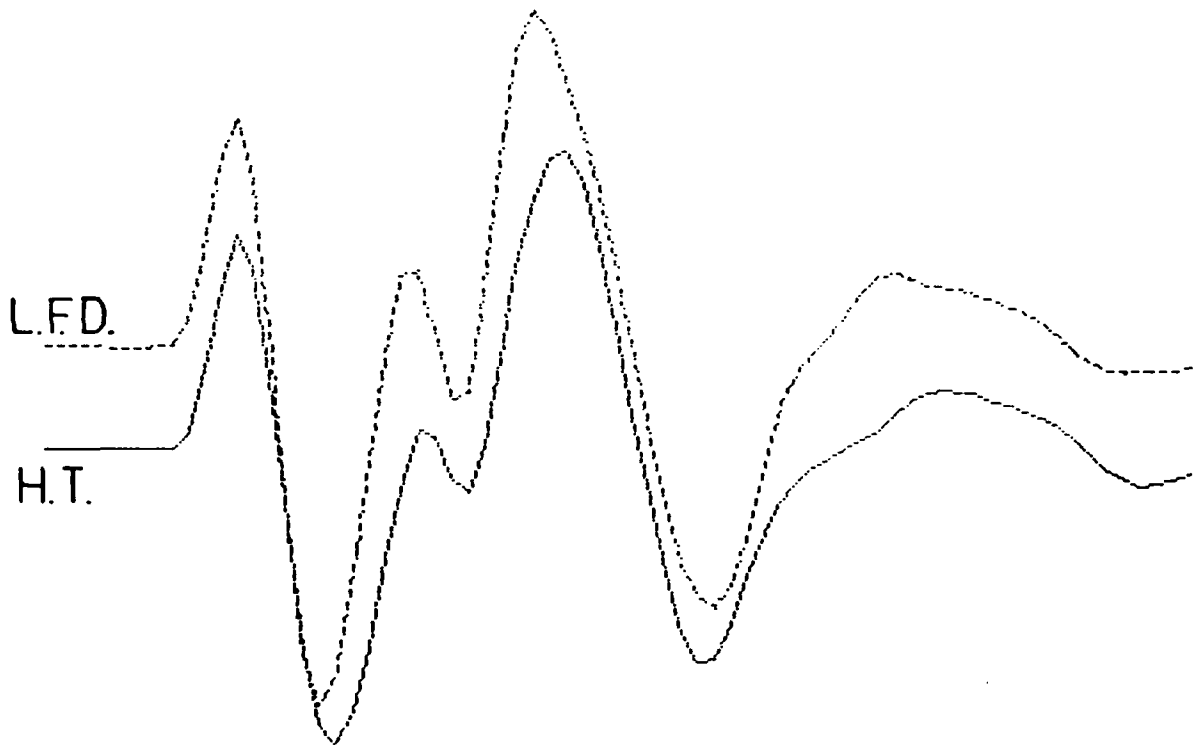
layered
 $\angle = 15^\circ$



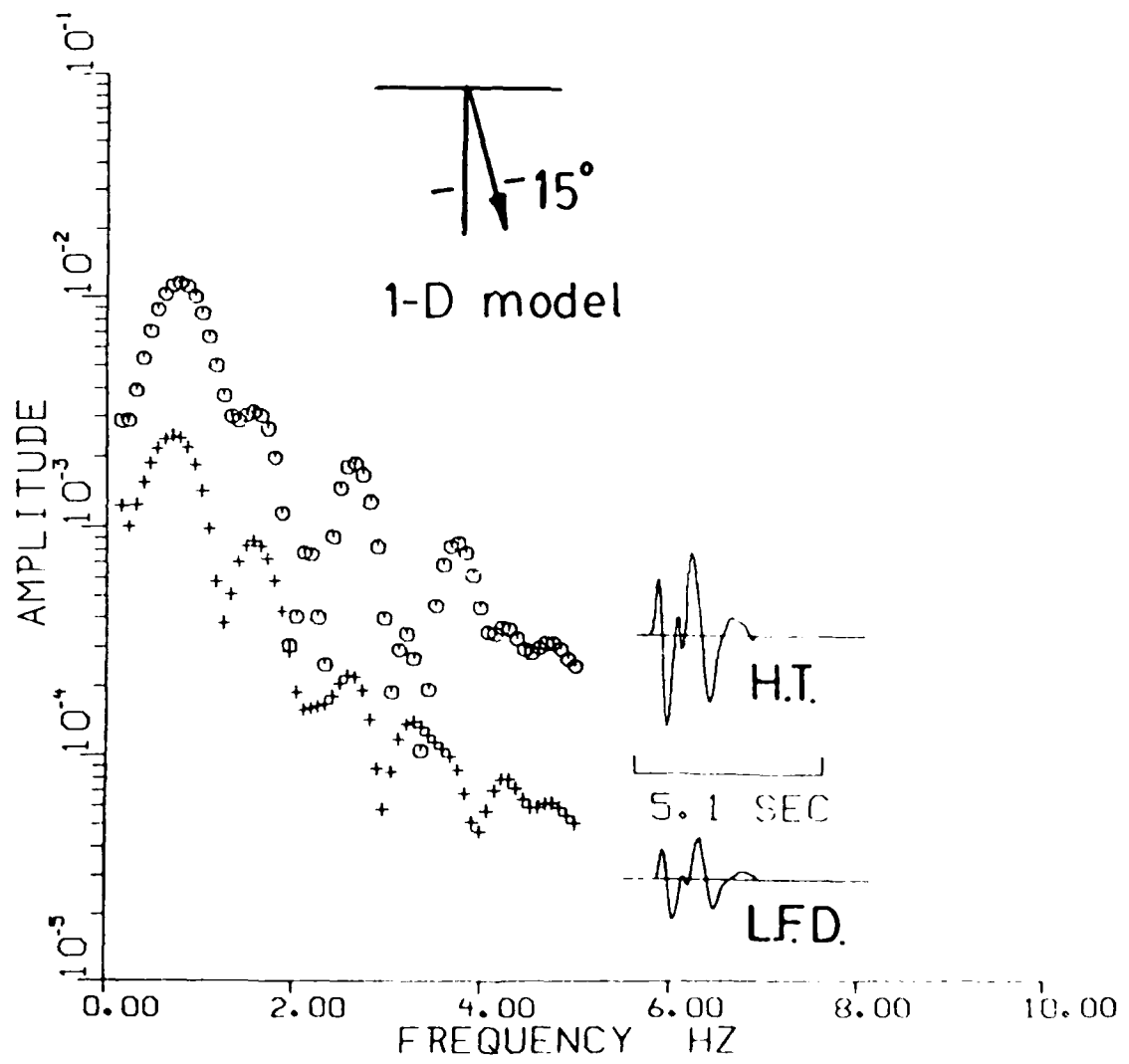


— YUCCA 1
- - - layered

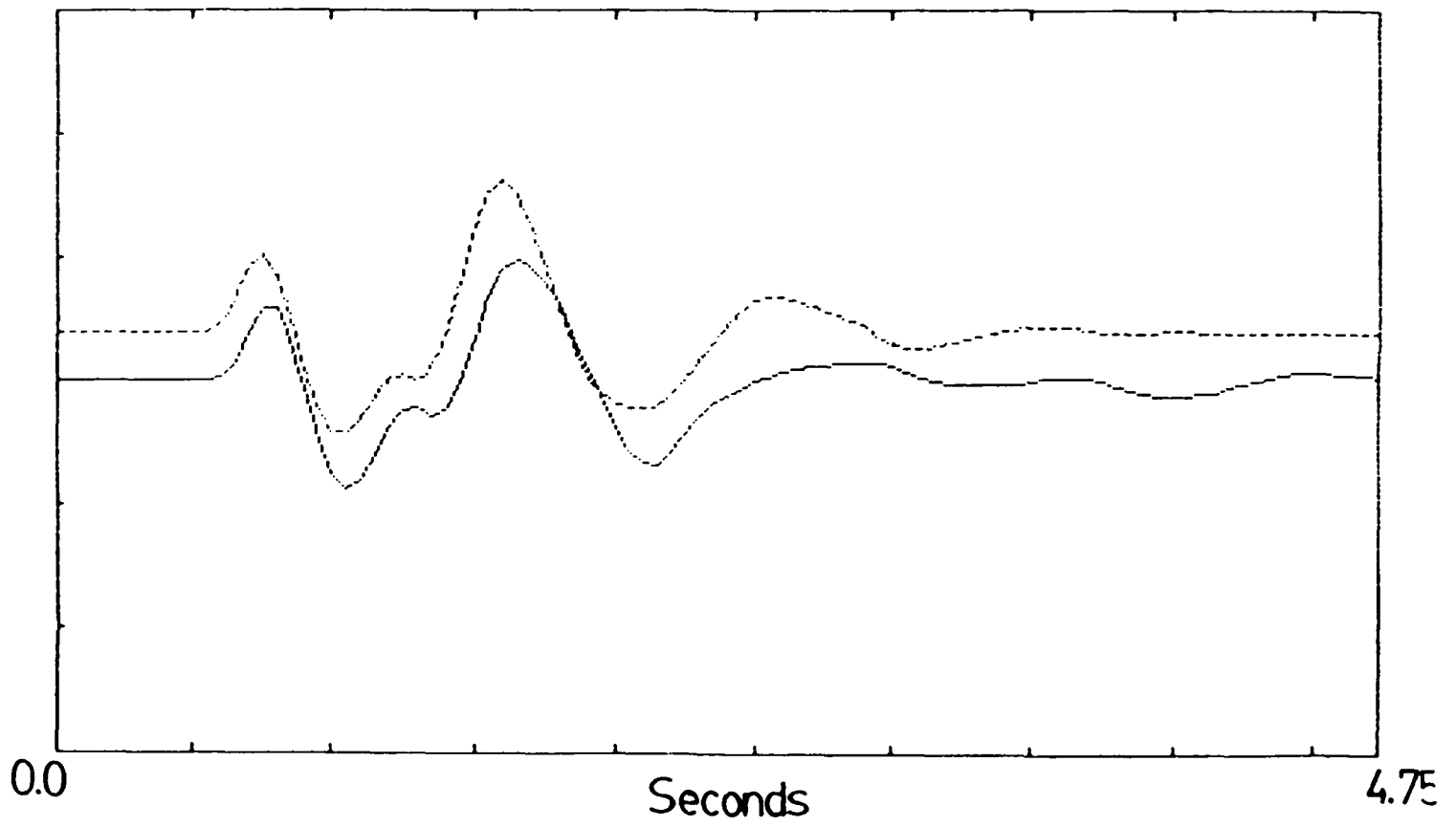
1-D model



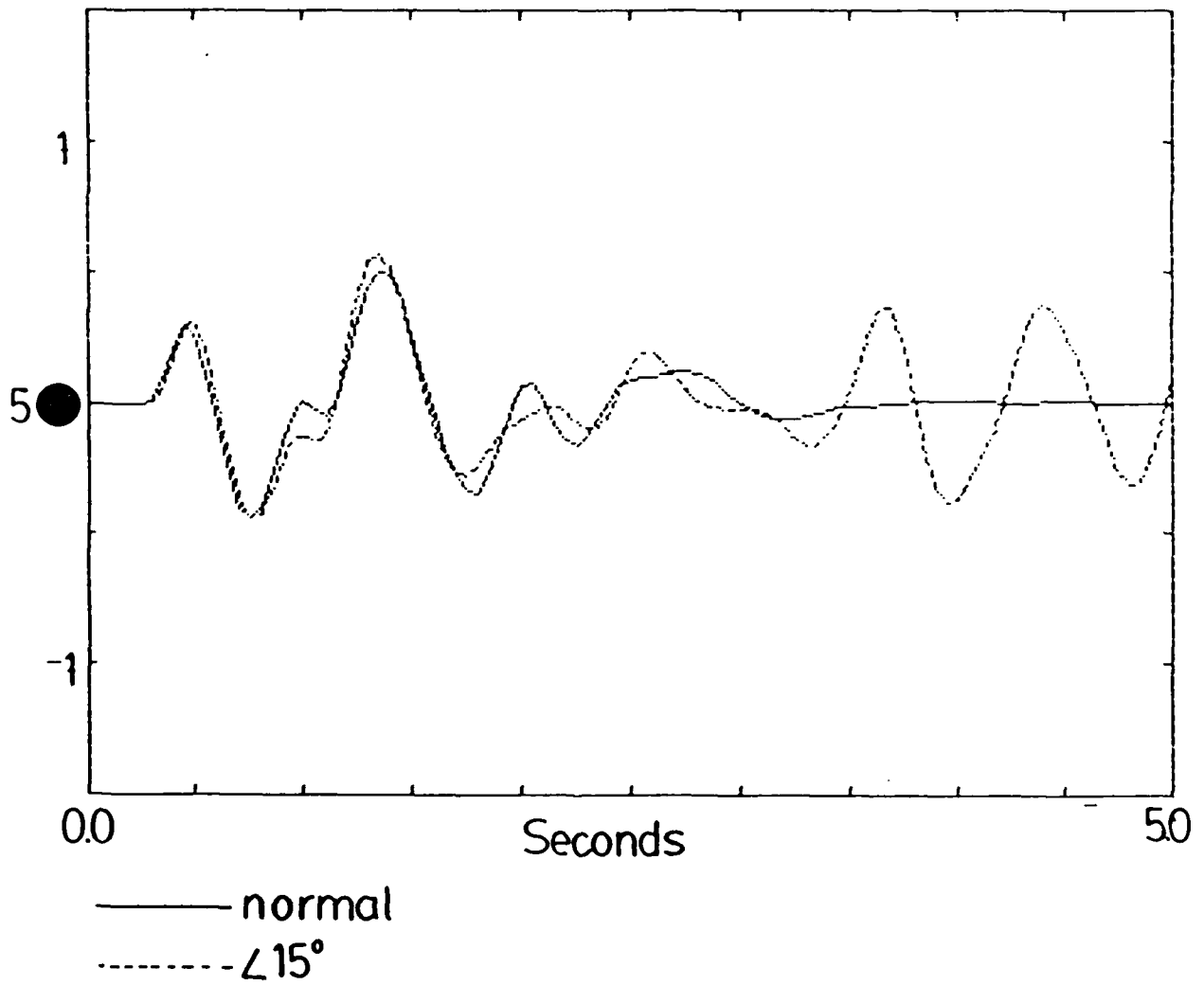
1.0 SEC



Layered Models



YUCCA 1



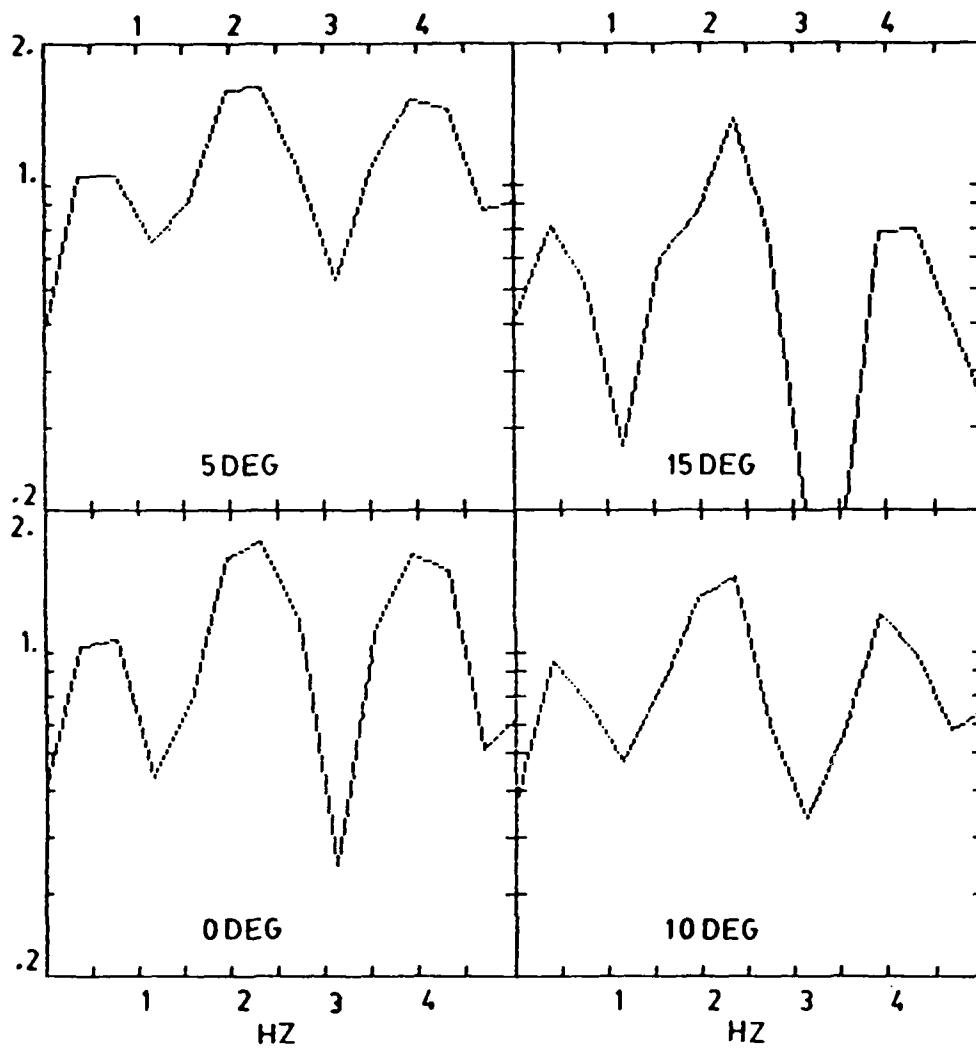


FIGURE 8

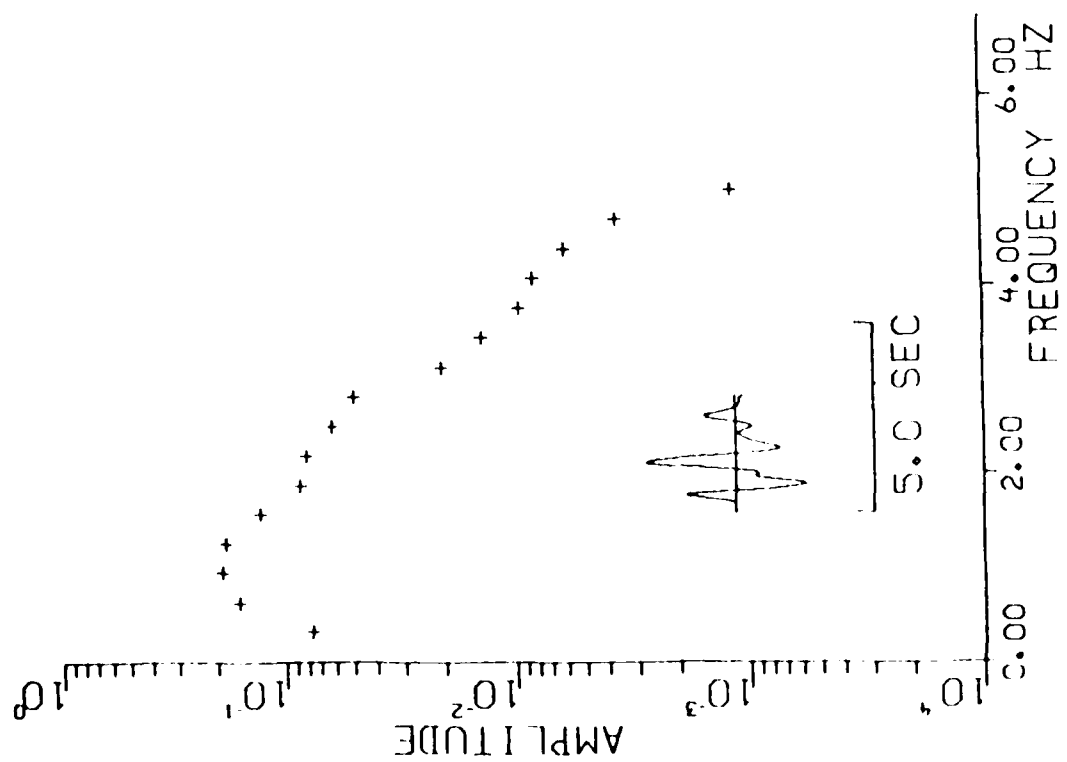
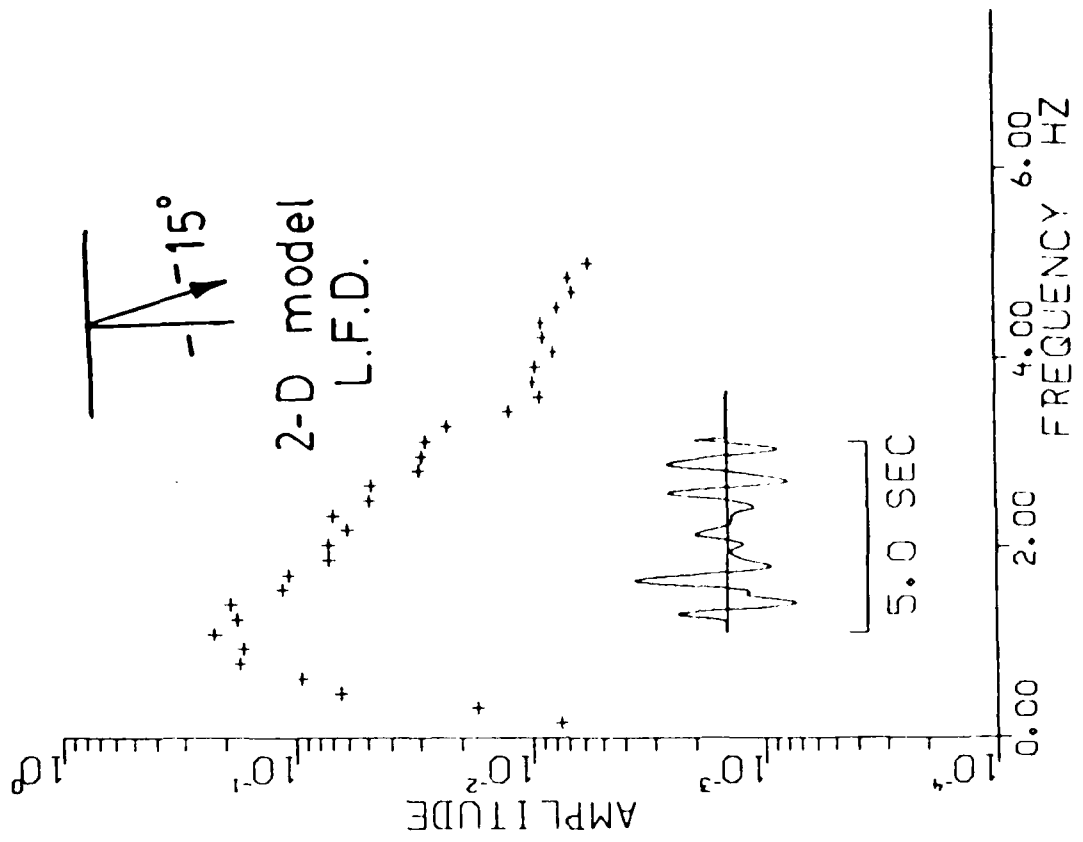
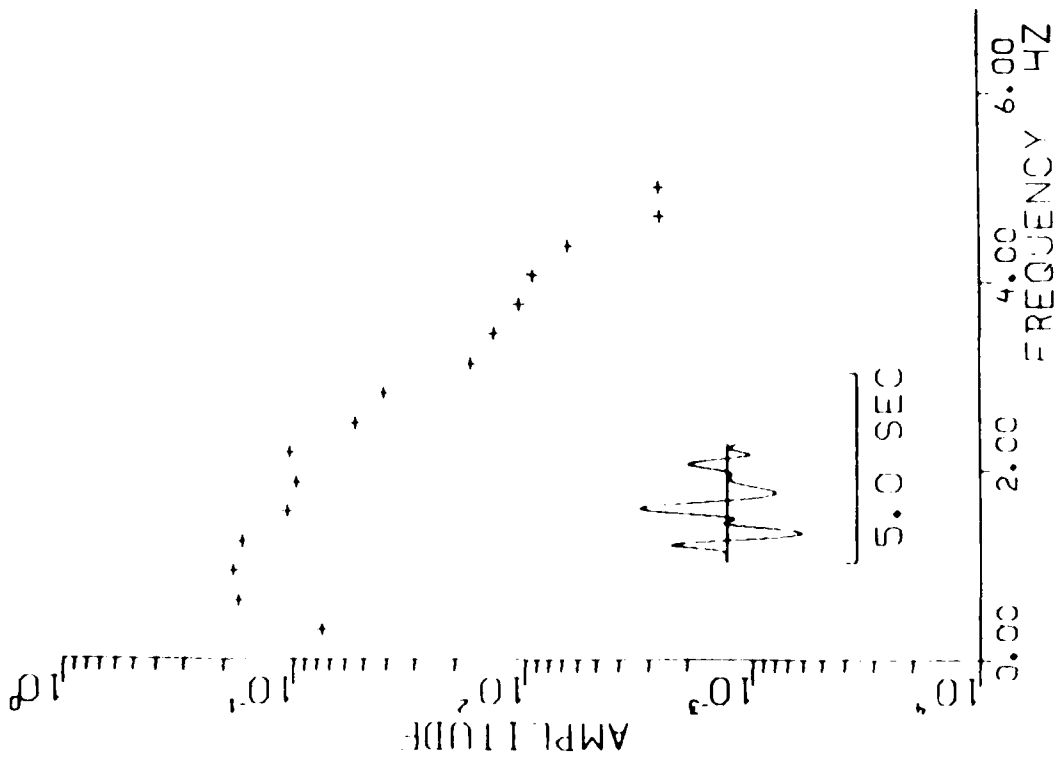
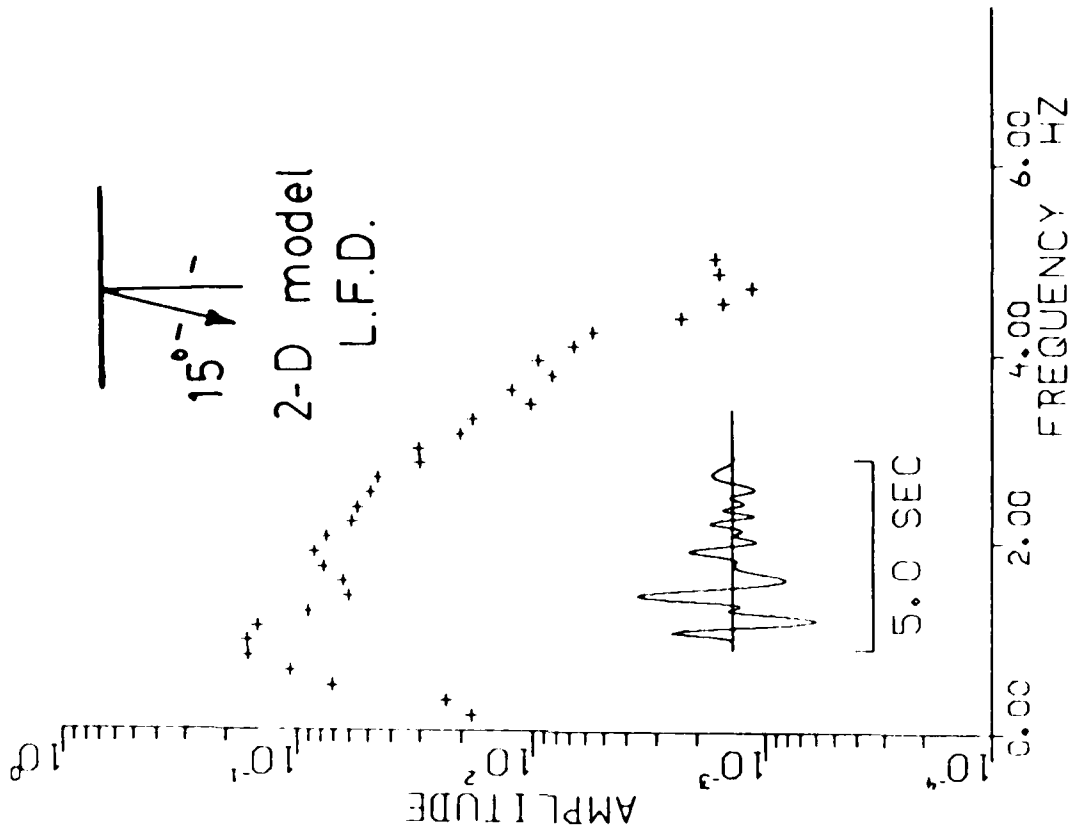
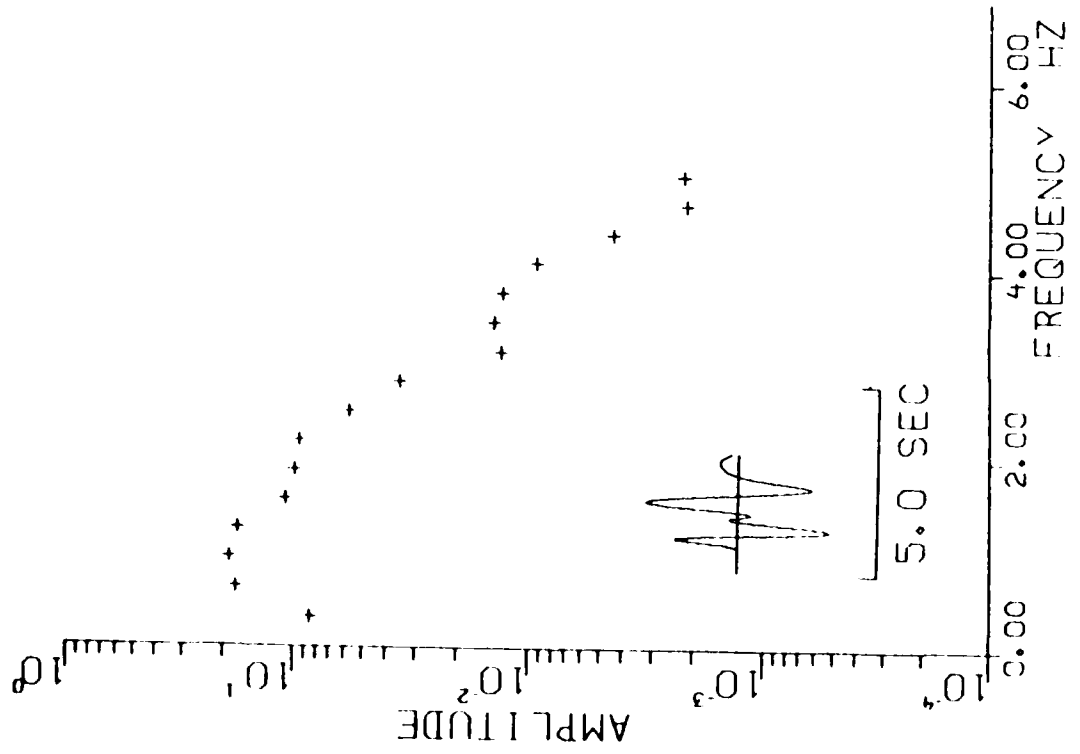
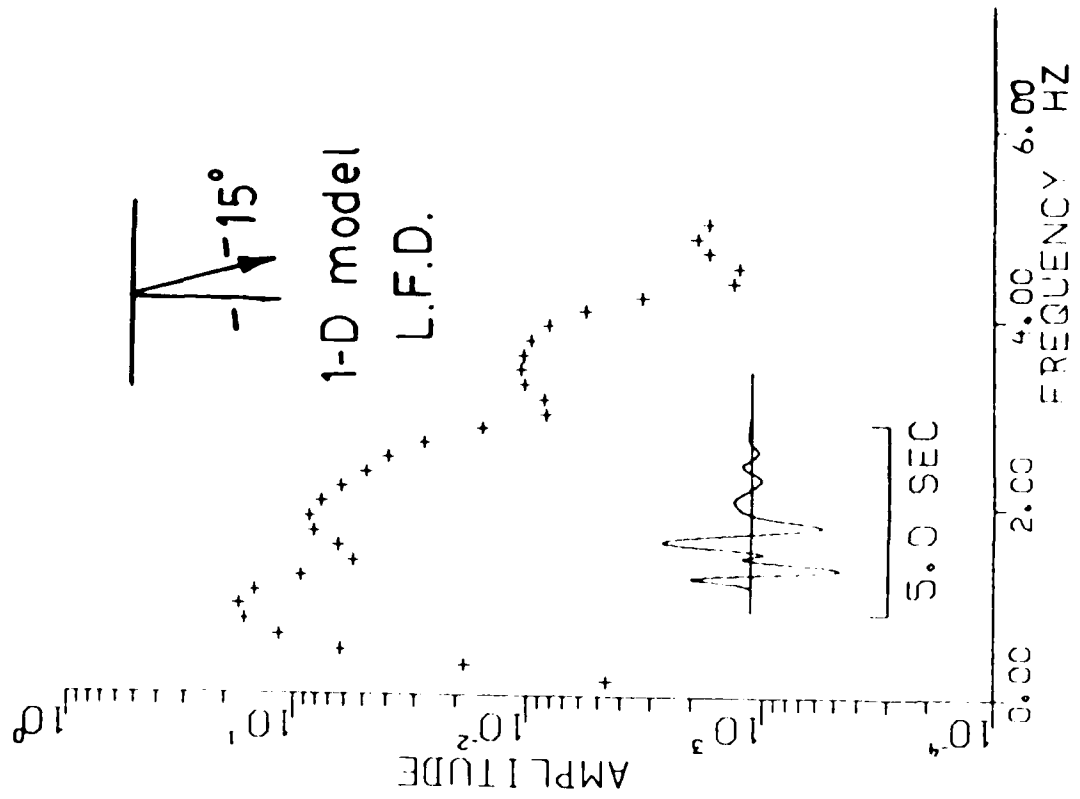
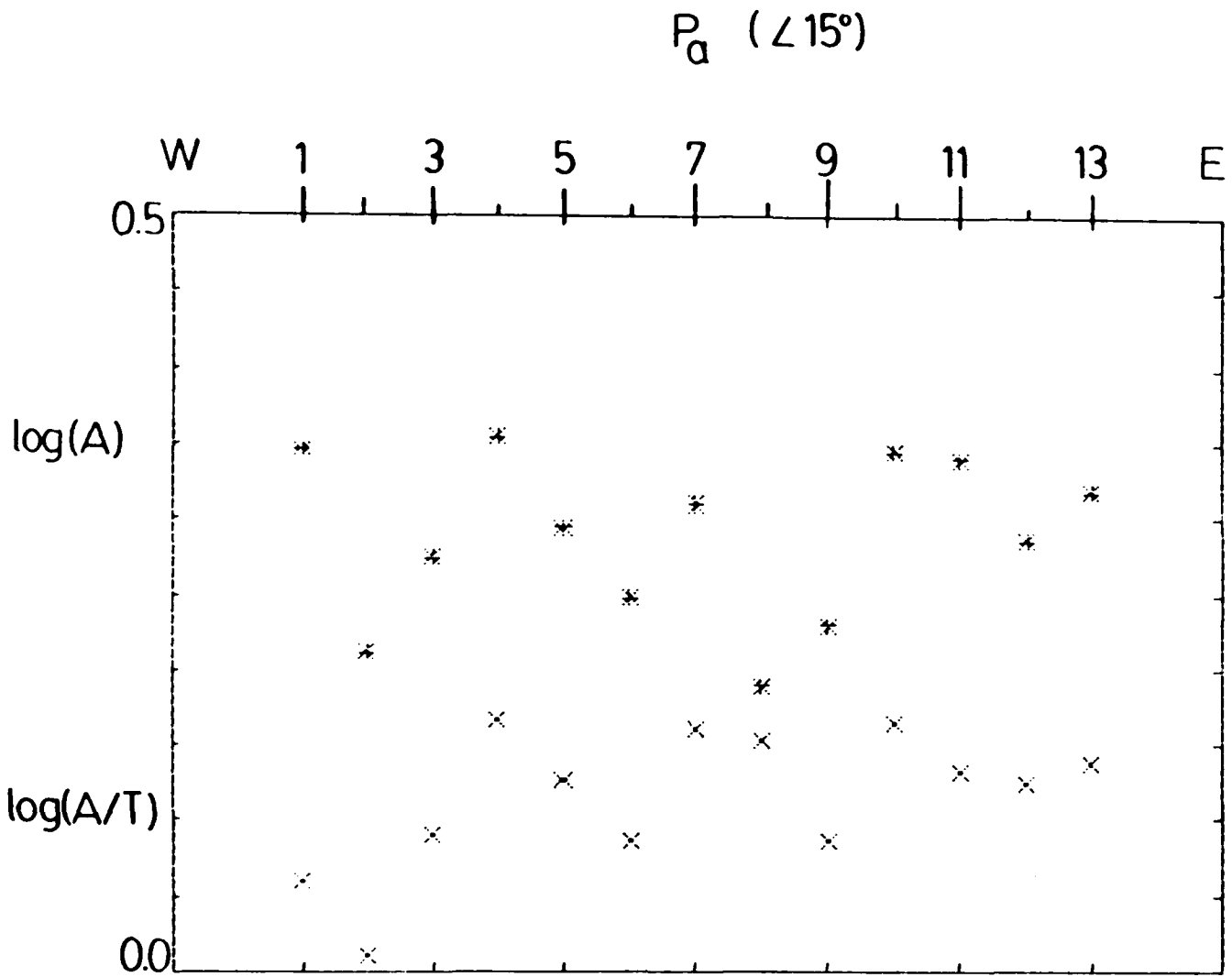


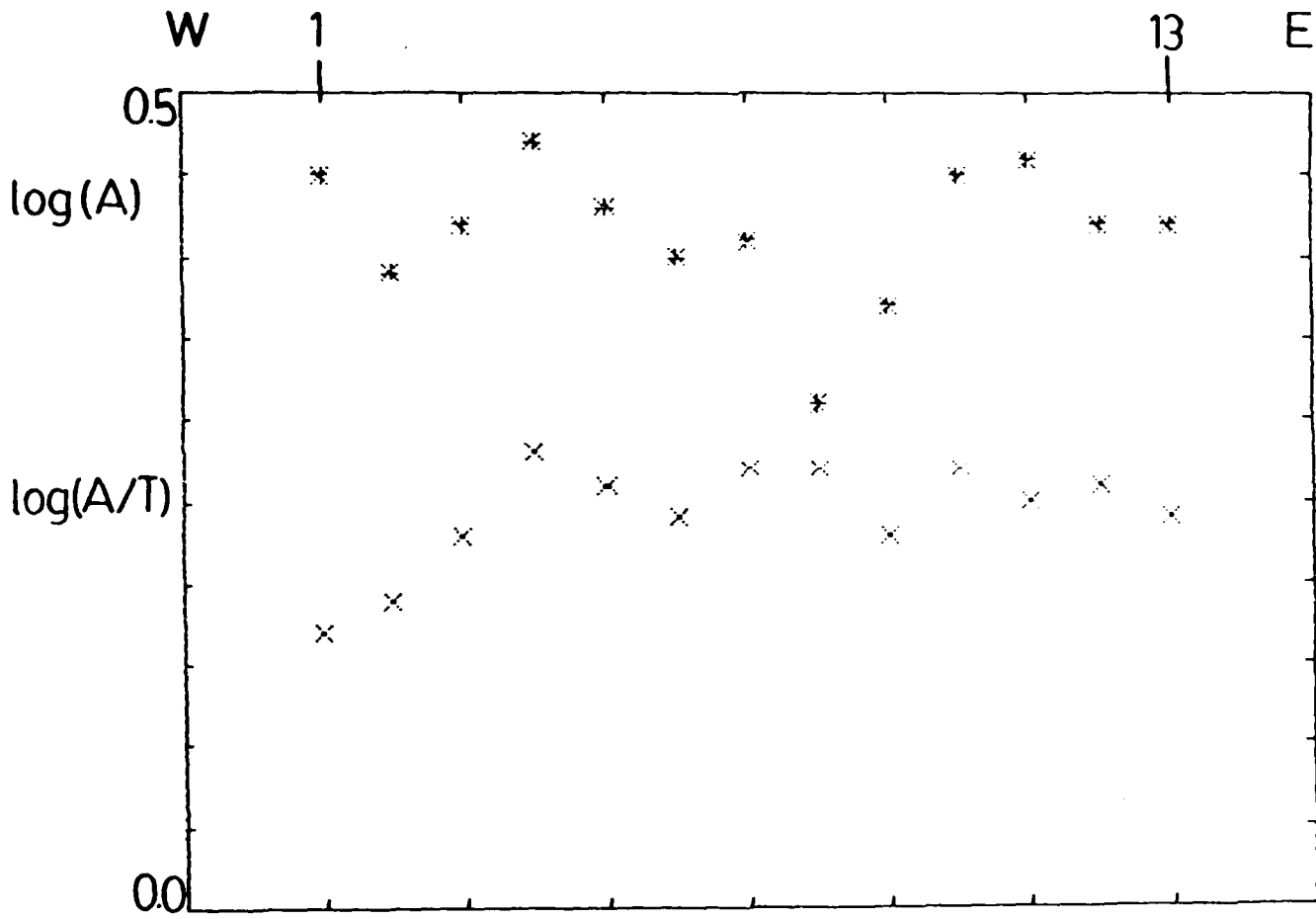
FIGURE 9A



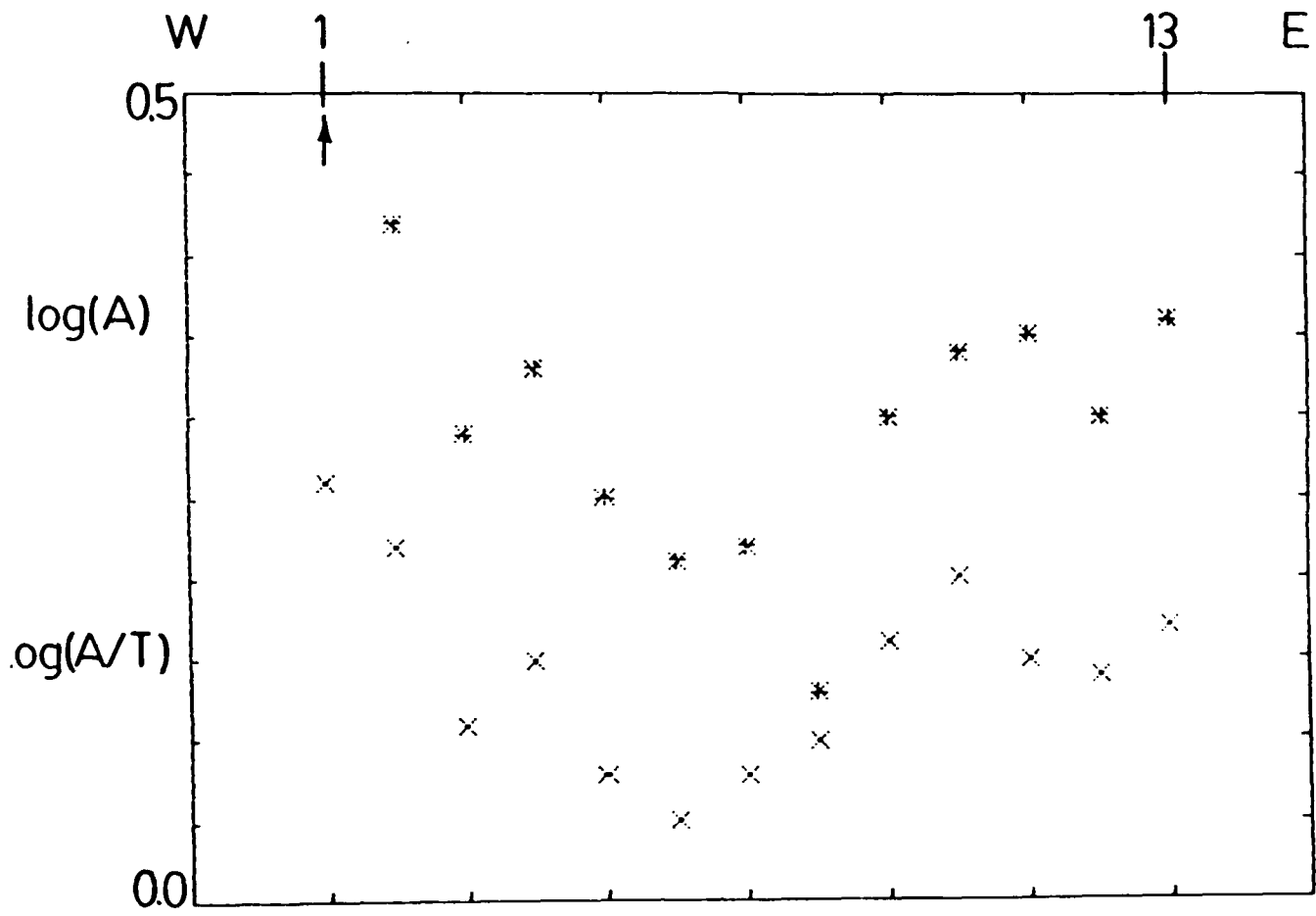




$P_b (\angle 15^\circ)$



$P_{\max} (\angle 15^\circ)$



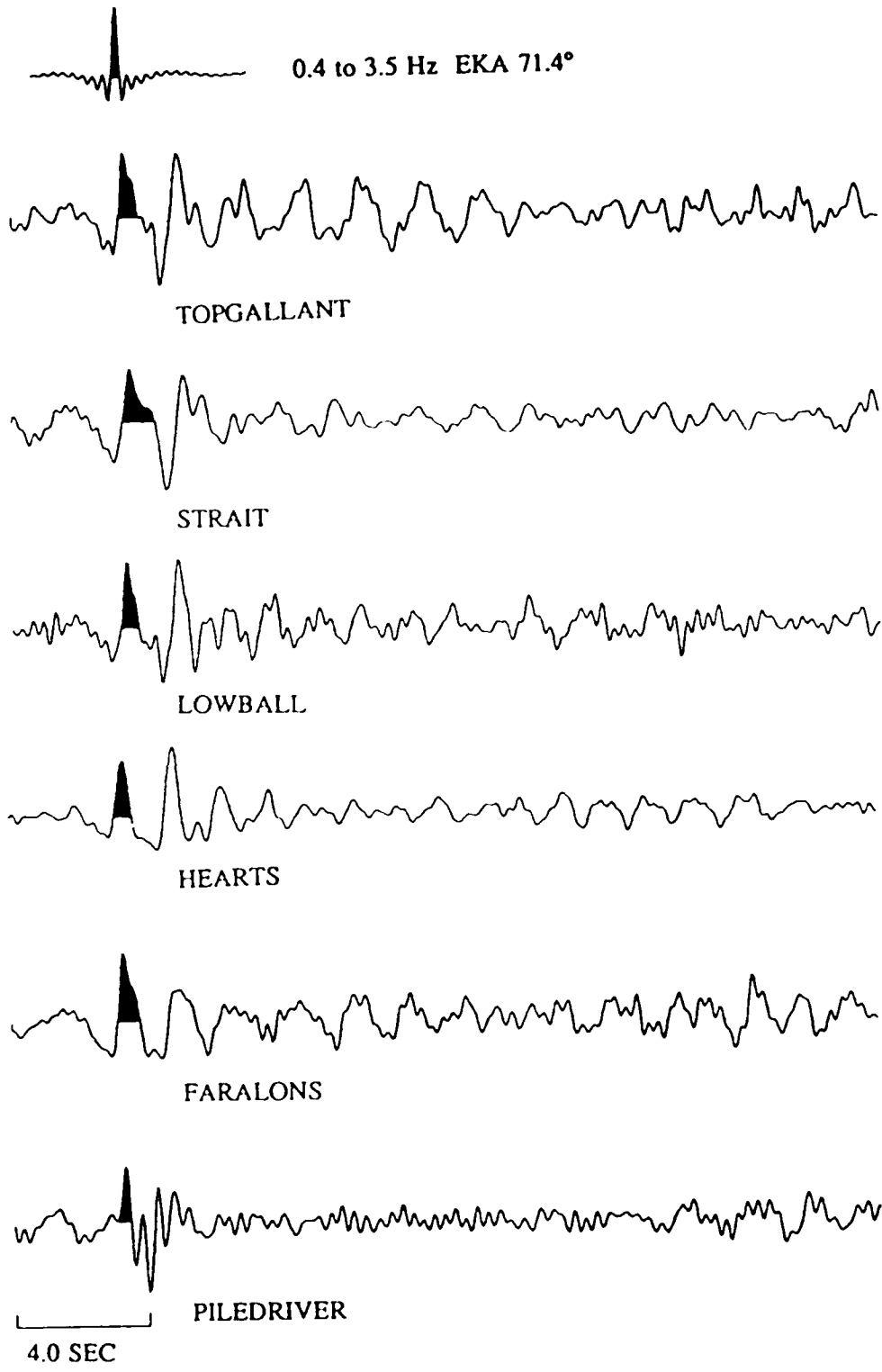


FIGURE 11A.



0.4 to 3.5 Hz YKA 25.5°



SCANTLING



TOPGALANT



QUARGEL



LOWBALL



CREWLINE



CABRILLO

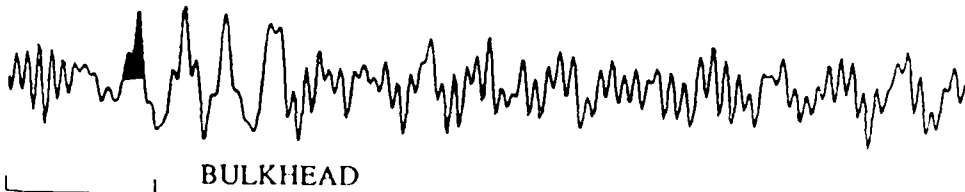
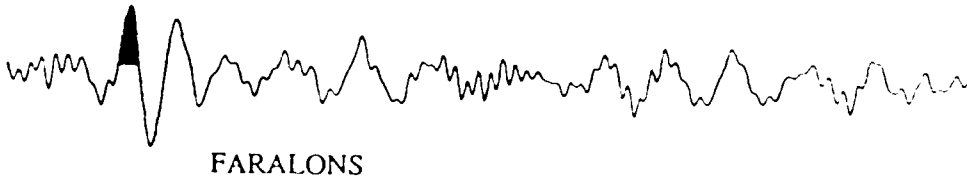


BULKHEAD

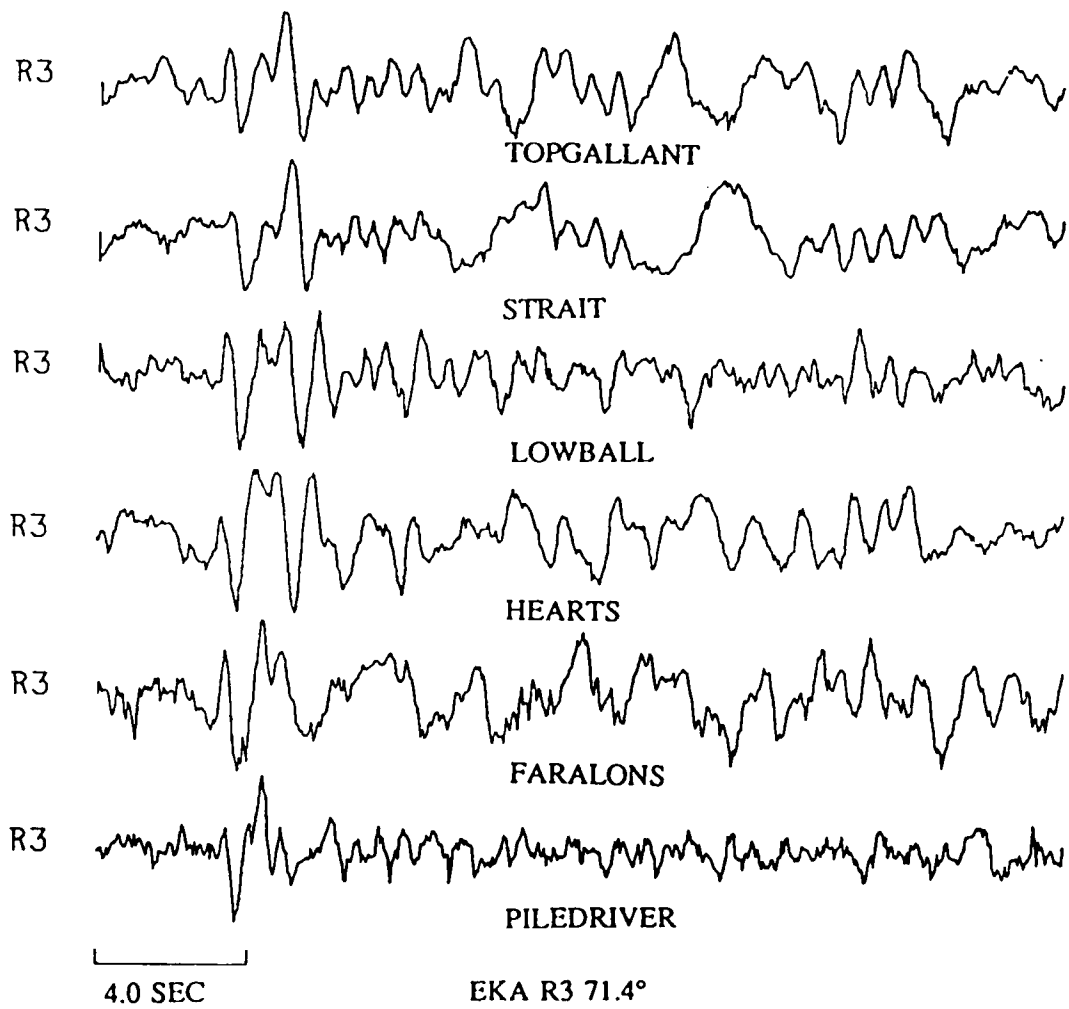
4.0 SEC



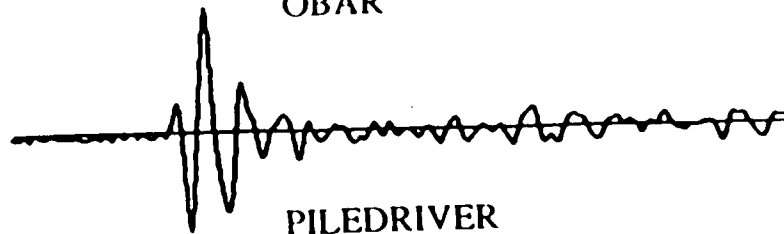
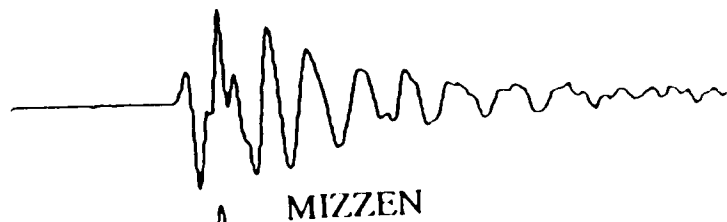
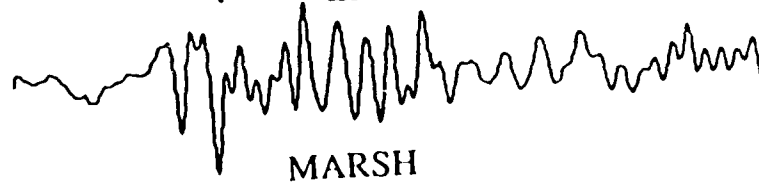
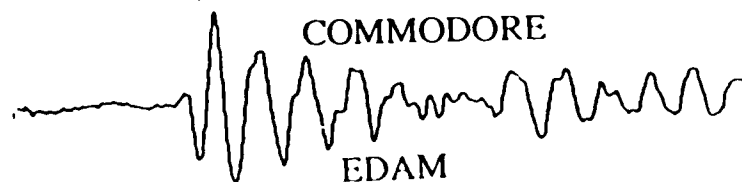
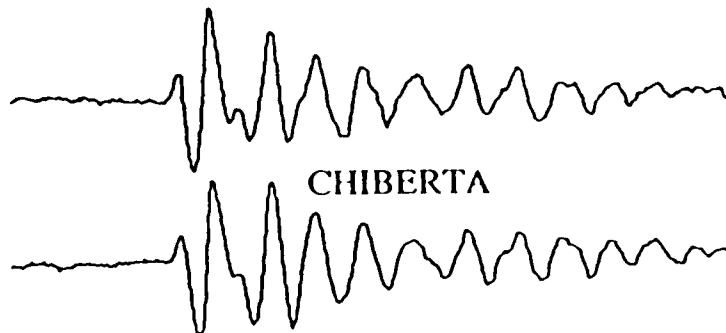
0.4 to 3.5 Hz GBA 127.8°



4.0 SEC



RK-ON 21.0°



5.0 SEC

DISTRIBUTION LIST

Dr. Monem Abdel-Cawad
Rockwell International Science Center
1049 Camino Dos Rios
Thousand Oaks, CA 91360

Professor Keliti Aki
Center for Earth Sciences
University of Southern California
University Park
Los Angeles, CA 90089-0741

Professor Shelton S. Alexander
Geosciences Department
403 Deike Building
The Pennsylvania State University
University Park, PA 16802

Professor Charles B. Archambeau
Cooperative Institute for Research in
Environmental Sciences
University of Colorado
Boulder, CO 80309

Dr. Thomas C. Bache Jr.
Science Applications Int'l Corp.
10210 Campus Point Drive
San Diego, CA 92121

Dr. James Bulau
Rockwell International Science Center
1049 Camino Dos Rios
P.O. Box 1085
Thousand Oaks, CA 91360

Dr. Douglas R. Baumgardt
Signal Analysis and Systems Division
ENSCO, Inc.
5400 Port Royal Road
Springfield, VA 22151-2388

Dr. S. Bratt
Science Applications Int'l Corp.
10210 Campus Point Drive
San Diego, CA 92121

Professor John Ebel
Department of Geology & Geophysics
Boston College
Chestnut Hill, MA 02167

Woodward-Clyde Consultants
Attn: Dr. Lawrence J. Burdick
Dr. Jeff Barker
P.O. Box 93245
Pasadena, CA 91109-3245 (2 copies)

Dr. Roy Burger
1221 Serry Rd.
Schenectady, NY 12309

Professor Robert W. Clayton
Seismological Laboratory
Division of Geological and Planetary
Sciences
California Institute of Technology
Pasadena, CA 91125

Dr. Vernon F. Cormier
Earth Resources Laboratory
Department of Earth, Atmospheric and
Planetary Sciences
Massachusetts Institute of Technology
42 Carleton Street
Cambridge, MA 02142

Professor Anton M. Dainty
Earth Resources Laboratory
Department of Earth, Atmospheric and
Planetary Sciences
Massachusetts Institute of Technology
42 Carleton Street
Cambridge, MA 02142

Dr. Zoltan A. Der
Teledyne Geotech
314 Montgomery Street
Alexandria, VA 22314

Prof. Adam Dziewonski
Hoffman Laboratory
Harvard University
20 Oxford St.
Cambridge, MA 02138

Professor John Ferguson
Center for Lithospheric Studies
The University of Texas at Dallas
P.O. Box 830688
Richardson, TX 75083-0688

Dr. Jeffrey W. Given
Sierra Geophysics
11255 Kirkland Way
Kirkland, WA 98033

Prof. Roy Greenfield
Geosciences Department
403 Deike Building
The Pennsylvania State University
University Park, PA 16802

Professor David G. Harkrider
Seismological Laboratory
Division of Geological and Planetary
Sciences
California Institute of Technology
Pasadena, CA 91125

Professor Donald V. HelMBERGER
Seismological Laboratory
Division of Geological and Planetary
Sciences
California Institute of Technology
Pasadena, CA 91125

Professor Eugene Herrin
Institute for the Study of Earth & Man
Geophysical Laboratory
Southern Methodist University
Dallas, TX 75275

Professor Robert B. Herrmann
Department of Earth and Atmospheric
Sciences
Saint Louis University
Saint Louis, MO 63156

Professor Lane R. Johnson
Seismographic Station
University of California
Berkeley, CA 94720

Professor Thomas H. Jordan
Department of Earth, Atmospheric and
Planetary Sciences
Massachusetts Institute of Technology
Cambridge, MA 02139

Dr. Alan Kafka
Department of Geology & Geophysics
Boston College
Chestnut Hill, MA 02167

Professor Charles A. Langston
Geosciences Department
403 Deike Building
The Pennsylvania State University
University Park, PA 16802

Professor Thorne Lay
Department of Geological Sciences
1006 C.C. Little Building
University of Michigan
Ann Arbor, MI 48109-1063

Dr. George R. Mellman
Sierra Geophysics
11255 Kirkland Way
Kirkland, WA 98033

Professor Brian J. Mitchell
Department of Earth and Atmospheric
Sciences
Saint Louis University
Saint Louis, MO 63156

Professor Thomas V. McEvelly
Seismographic Station
University of California
Berkeley, CA 94720

Dr. Keith L. McLaughlin
Teledyne Geotech
314 Montgomery Street
Alexandria, VA 22314

Professor Otto W. Nuttli
Department of Earth and Atmospheric
Sciences
Saint Louis University
Saint Louis, MO 63156

Professor Paul G. Richards
Lamont-Doherty Geological Observatory
of Columbia University
Palisades, NY 10964

Dr. Norton Rimer
S-Cubed
A Division of Maxwell Laboratory
P.O. 1620
La Jolla, CA 92038-1620

Professor Larry J. Ruff
Department of Geological Sciences
1006 C.C. Little Building
University of Michigan
Ann Arbor, MI 48109-1063

Professor Charles G. Sammis
Center for Earth Sciences
University of Southern California
University Park
Los Angeles, CA 90089-0741

Dr. David G. Simpson
Lamont-Doherty Geological Observatory
of Columbia University
Palisades, NY 10964

Dr. Jeffrey L. Stevens
S-CUBED,
A Division of Maxwell Laboratory
P.O. Box 1620
La Jolla, CA 92038-1620

Professor Brian Stump
Institute for the Study of Earth
and Man
Geophysical Laboratory
Southern Methodist University
Dallas, TX 75275

Professor Ta-liang Teng
Center for Earth Sciences
University of Southern California
University Park
Los Angeles, CA 90089-0741

Dr. R. B. Tittmann
Rockwell International Science Center
1049 Camino Dos Rios
P.O. Box 1085
Thousand Oaks, CA 91360

Professor M. Nafi Toksoz
Earth Resources Laboratory
Department of Earth, Atmospheric and
Planetary Sciences
Massachusetts Institute of Technology
42 Carleton Street
Cambridge, MA 02142

Professor Terry C. Wallace
Department of Geosciences
Building #11
University of Arizona
Tucson, AZ 85721

Prof. John H. Woodhouse
Hoffman Laboratory
Harvard University
20 Oxford St.
Cambridge, MA 02138

Dr. G. Blake
US Dept. of Energy/DP 331
Forrestal Building
1000 Independence Ave.
Washington, D.C. 20585

Dr. Michel Bouchon
Universite Scientifique et
Medicale de Grenoble
Laboratoire de Geophysique
Interne et Tectonophysique
I.R.I.G.M.-B.P. 68
38402 St. Martin D'Herès
Cedex FRANCE

Dr. Hilmar Bungum
NTNF/NORSAR
P.O. Box 51
Norwegian Council of Science,
Industry and Research, NORSAR
N-2007 Kjeller, NORWAY

Dr. Alan Douglas
Ministry of Defense
Blacknest, Brimpton, Reading RG7-4RS
UNITED KINGDOM

Professor Peter Harjes
Institute for Geophysik
Rhur University
Bochum
P.O. Box 102148
4630 Bochum 1
FEDERAL REPUBLIC OF GERMANY

Dr. James Hannon
Lawrence Livermore National Laboratory
P.O. Box 808
Livermore, CA 94550

Dr. E. Husebye
NTNF/NORSAR
P.O. Box 51
N-2007 Kjeller, NORWAY

Dr. Arthur Lerner-Lam
Lamont-Doherty Geological Observatory
of Columbia University
Palisades, NY 10964

Mr. Peter Marshall
Procurement Executive
Ministry of Defense
Blacknest, Brimpton, Reading RG7-4RS
UNITED KINGDOM

Dr. B. Massinon
Societe Radiomana
27, Rue Claude Bernard
75005, Paris, FRANCE

Dr. Pierre Mechler
Societe Radiomana
27, Rue Claude Bernard
75005, Paris, FRANCE

Mr. Jack Murphy
S-CUBED
Reston Geophysics Office
11800 Sunrise Valley Drive
Suite 1212
Reston, VA 22091

Dr. Svein Mykkeltveit
NTNF/NORSAR
P.O. Box 51
N-2007 Kjeller, NORWAY

Dr. Carl Newton
Los Alamos National Laboratory
P.O. Box 1663
Mail Stop C 335, Group ESS3
Los Alamos, NM 87545

Dr. Peter Basham
Earth Physics Branch
Department of Energy and Mines
1 Observatory Crescent
Ottawa, Ontario
CANADA K1A 0Y3

Professor J. A. Orcutt
Geological Sciences Division
Univ. of California at San Diego
La Jolla, CA 92093

Dr. Frank F. Pilotte
Director of Geophysics
Headquarters Air Force Technical
Applications Center
Patrick AFB, Florida 32925-6001

Professor Keith Priestley
University of Nevada
Mackay School of Mines
Reno, Nevada 89557

Mr. Jack Raclin
USGS - Geology, Rm 3C136
Mail Stop 928 National Center
Reston, VA 22092

Dr. Frode Ringdal
NTNF/NORSAR
P.O. Box 51
N-2007 Kjeller, NORWAY

Dr. George H. Rothe
Chief, Research Division
Geophysics Directorate
Headquarters Air Force Technical
Applications Center
Patrick AFB, Florida 32925-6001

Dr. Alan S. Ryall, Jr.
Center for Seismic Studies
1300 North 17th Street
Suite 1450
Arlington, VA 22209-2308

Dr. Jeffrey L. Stevens
S-CUBED,
A Division of Maxwell Laboratory
P.O. Box 1620
La Jolla, CA 92038-1620

Dr. Lawrence Turnbull
OSWR/NED
Central Intelligence Agency
CIA, Room 5G48
Washington, DC 20505

Professor Steven Grand
Department of Geology
245 Natural History Bldg
1301 West Green Street
Urbana, IL 61801

Teledyne Geotech Alexandria Laboratory
Attn: K. L. McLaughlin
314 Montgomery Street
Alexandria, VA 22314

10 copies

DARPA/PM
1400 Wilson Boulevard
Arlington, VA 22209

U.S. Geological Survey
ATTN: Dr. T. Hanks
National Earthquake Research Center
345 Middlefield Road
Menlo Park, CA 94025

Defense Technical Information Center
Cameron Station
Alexandria, VA 22314 (12 copies)

SRI International
333 Ravensworth Avenue
Menlo Park, CA 94025

Defense Intelligence Agency
Directorate for Scientific and
Technical Intelligence
Washington, D.C. 20301

Center for Seismic Studies
ATTN: Dr. C. Romney
1300 North 17th Street
Suite 1450
Arlington, VA 22209 (3 copies)

Defense Nuclear Agency
Shock Physics Directorate/SS
Washington, D.C. 20305

Dr. Robert Blandford
DARPA/GSD
1400 Wilson Boulevard
Arlington, VA 22209-2308

Defense Nuclear Agency/SPSS
ATTN: Dr. Michael Shore
6801 Telegraph Road
Alexandria, VA 22310

Ms. Ann Kerr
DARPA/GSD
1400 Wilson Boulevard
Arlington, VA 22209-2308

AFOSR/NPG
ATTN: Director
Bldg 410, Room C222
Bolling AFB, Washington, D.C. 20332

Dr. Ralph Alewine III
DARPA/GSD
1400 Wilson Boulevard
Arlington, VA 22209-2308

AFTAC/CA (STINFO)
Patrick AFB, FL 32925-6001

Mr. Edward Giller
Pacific Sierra Research Corp.
1401 Wilson Boulevard
Arlington, VA 22209

AFWL/NTESC
Kirtland AFB, NM 87171

Science Horizons, Inc.
Attn: Dr. Bernard Minster
Dr. Theodore Cherry
710 Encinitas Blvd., Suite 101
Encinitas, CA 92024 (2 copies)

U.S. Arms Control & Disarmament Agency
ATTN: Mrs. M. Hoinkes
Div. of Multilateral Affairs, Rm 5499
Washington, D.C. 20451

Dr. Jack Evernden
USGS - Earthquake Studies
345 Middlefield Road
Menlo Park, CA 94025

Dr. Lawrence Braille
Department of Geosciences
Purdue University
West Lafayette, IN 47907

Dr. G.A. Bollinger
Department of Geological Sciences
Virginia Polytechnical Institute
21044 Derring Hall
Blacksburg, VA 24061

Dr. L. Sykes
Lamont Doherty Geological Observatory
Columbia University
Palisades, NY 10964

Dr. S.W. Smith
Geophysics Program
University of Washington
Seattle, WA 98195

Dr. L. Timothy Long
School of Geophysical Sciences
Georgia Institute of Technology
Atlanta, GA 30332

Dr. N. Biswas
Geophysical Institute
University of Alaska
Fairbanks, AK 99701

Dr. Freeman Gilbert
Institute of Geophysics &
Planetary Physics
Univ. of California at San Diego
P.O. Box 109
La Jolla, CA 92037

Dr. Pradeep Talwani
Department of Geological Sciences
University of South Carolina
Columbia, SC 29208

University of Hawaii
Institute of Geophysics
Attn: Dr. Daniel Walker
Honolulu, HI 96822

Dr. Donald Forsyth
Department of Geological Sciences
Brown University
Providence, RI 02912

Dr. Jack Oliver
Department of Geology
Cornell University
Ithaca, NY 14850

Dr. Muawia Barazangi
Geological Sciences
Cornell University
Ithaca, NY 14853

Rondout Associates
Attn: Dr. George Sutton
Dr. Jerry Carter
Dr. Paul Pomeroy
P.O. Box 224
Stone Ridge, NY 12484 (3 copies)

Dr. M. Sorrells
Geotech/Teledyne
P.O. Box 28277
Dallas, TX 75228

Dr. Bob Smith
Department of Geophysics
University of Utah
1400 East 2nd South
Salt Lake City, UT 84112

Dr. Anthony Gangi
Texas A&M University
Department of Geophysics
College Station, TX 77843

Dr. Gregory B. Young
ENSCO, Inc.
5400 Port Royal Road
Springfield, CA 22151

Dr. Ben Menaheim
Weizman Institute of Science
Rehovot, ISRAEL 951729

Weidlinger Associates
Attn: Dr. Gregory Wojcik
620 Hansen Way, Suite 100
Palo Alto, CA 94304

Dr. Leon Knopoff
University of California
Institute of Geophysics & Planetary
Physics
Los Angeles, CA 90024

Dr. Kenneth H. Olsen
Los Alamos Scientific Laboratory
Post Office Box 1663
Los Alamos, NM 87545

Prof. Jon F. Claerbout
Prof. Amos Nur
Dept. of Geophysics
Stanford University
Stanford, CA 94305 (2 copies)

AFGL/XO
Hanscom AFB, MA 01731-5000

Dr. Robert Burrige
Schlumberger-Doll Research Ctr.
Old Quarry Road
Ridgefield, CT 06877

AFGL/LW
Hanscom AFB, MA 01731-5000

Dr. Eduard Berg
Institute of Geophysics
University of Hawaii
Honolulu, HI 96822

AFGL/SULL
Research Library
Hanscom AFB, MA 01731-5000 (2 copies)

Secretary of the Air Force (SAFRD)
Washington, DC 20330

Dr. Robert Phinney
Dr. F.A. Dahlen
Dept. of Geological & Geophysical Sci.
Princeton University
Princeton, NJ 08540 (2 copies)

Office of the Secretary Defense
DDR & E
Washington, DC 20330

Dr. Kin-Yip Chun
Geophysics Division
Physics Department
University of Toronto
Ontario, CANADA M5S 1A7

HQ DNA
Attn: Technical Library
Washington, DC 20305

New England Research, Inc.
Attn: Dr. Randolph Martin III
P.O. Box 857
Norwich, VT 05055

Director, Technical Information
DARPA
1400 Wilson Blvd.
Arlington, VA 22209

Sandia National Laboratory
Attn: Dr. H.B. Durham
Albuquerque, NM 87185

Los Alamos Scientific Laboratory
Attn: Report Library
Post Office Box 1663
Los Alamos, NM 87544

Dr. Gary McCartor
Mission Research Corp.
735 State Street
P. O. Drawer 719
Santa Barbara, CA 93102

Dr. Thomas Weaver
Los Alamos Scientific Laboratory
Los Alamos, NM 87544

Dr. W. H. K. Lee
USGS
Office of Earthquakes, Volcanoes,
& Engineering
Branch of Seismology
345 Middlefield Rd
Menlo Park, CA 94025

Dr. Al Florence
SRI International
333 Ravenswood Avenue
Menlo Park, CA 94025-3493

END

5-87

DTIC